

# Soft X-ray properties of a spectroscopically selected sample of interacting and isolated Seyfert galaxies <sup>\*</sup>

F. Pfefferkorn<sup>1</sup>, Th. Boller<sup>1</sup> and P. Rafanelli<sup>2</sup>

<sup>1</sup> Max-Planck-Institut für extraterrestrische Physik, Postfach 1312, 85741 Garching, Germany

<sup>2</sup> Department of Astronomy, University of Padova, Vicolo Osservatorio 5, 35122 Padova, Italy

Received: 11 October 2000; Accepted: 09 January 2001

**Abstract.** We present a catalogue of ROSAT detected sources in the sample of spectroscopically selected Seyfert 1 and Seyfert 2 galaxies of Rafanelli et al. (1995). The catalogue contains 102 Seyfert 1 and 36 Seyfert 2 galaxies. The identification is based on X-ray contour maps overlaid on optical images taken from the Digitized Sky Survey. We have derived the basic spectral and timing properties of the X-ray detected Seyfert galaxies. For Seyfert 1 galaxies a strong correlation between photon index and X-ray luminosity is detected. We confirm the presence of generally steeper X-ray continua in narrow-line Seyfert 1 galaxies (NLS1s) compared to broad-line Seyfert 1 galaxies. Seyfert 2 galaxies show photon indices similar to those of NLS1s. Whereas a tendency for an increasing X-ray luminosity with increasing interaction strength is found for Seyfert 1 galaxies, such a correlation is not found for Seyfert 2 galaxies. For Seyfert 1 galaxies we found also a strong correlation for increasing far-infrared luminosity with increasing interaction strength. Both NLS1s and Seyfert 2 galaxies show the highest values of far-infrared luminosity compared to Seyfert 1 galaxies, suggesting that NLS1s and Seyfert 2 galaxies host strong (circumnuclear) starformation. For variable Seyfert galaxies we present the X-ray light curves obtained from the ROSAT All-Sky Survey and from ROSAT PSPC and HRI pointed observations. Besides the expected strong short- and long-term X-ray variability in Seyfert 1 galaxies, we find indications for X-ray flux variations in Seyfert 2 galaxies.

**Key words.** Catalogs – Galaxies: active – Galaxies: interactions – Galaxies: Seyfert – X-rays: galaxies

## 1. Introduction

Interaction between galaxies is considered to have a wide importance in triggering starburst and AGN activity, which is thought to produce a rise in the luminosity.

Several studies of physical mechanisms which could trigger a burst of strong star formation have been investigated by Barnes & Hernquist (1991, 1996), Jog & Das (1992), Jog & Solomon (1992) and Mihos & Hernquist (1996).

Also many observations suggest that galactic encounters enhance star formation rates, as demonstrated by studies of the optical (e.g., Kennicutt et al. 1987; Bushouse 1987), infrared (e.g., Bernlöhr 1993; Telesco et al. 1993) and radio (e.g., Hummel 1981; Smith & Kassim 1993) emission from interacting systems. In the X-ray band, an enhanced starburst activity will result in an increase in the X-ray luminosity due to the enhanced supernova rate. In addition, galaxy interaction might cause an increase

in the accretion rate onto the black hole, resulting in an additional increase in the X-ray luminosity.

We have investigated the X-ray properties of a spectroscopically selected sample of Seyfert 1, NLS1 and Seyfert 2 galaxies with  $z < 0.11$ ,  $m_v \leq 15.5$  and  $\delta \geq -23^\circ$  (Rafanelli et al., 1995). The physical pairs have been selected on POSS plates using the following criteria: separation between components  $S < 3D_p$ , where  $D_p$  is the apparent major axis of the Seyfert galaxy, and magnitude-difference between Seyfert galaxy and companion  $\Delta m_v = m_{v,comp} - m_{v,Seyfert} < 3$  (Rafanelli et al., 1995). Approximately 30 % of the ROSAT detected sources within the Rafanelli sample are Seyfert galaxies with separated physical companions, 32 Seyfert 1 and 11 Seyfert 2 galaxies match the criteria mentioned above. Some of the isolated sources with a disturbed morphology are probably merging galaxies or very close pairs, for which no separation  $S$  is given by Rafanelli et. al. (1995).

The aim of this paper is to present the timing and spectral X-ray properties of Seyfert 1, NLS1 and Seyfert 2 galaxies. In Sect. 2 we describe the X-ray data analysis as well as the identification process. The spectral features

Send offprint requests to: F. Pfefferkorn, pfefferk@mpe.mpg.de

<sup>\*</sup> All overlays can be retrieved via CDS anonymous ftp 130.79.128.5

and timing results, including the relation between the interaction strength  $Q$  and the X-ray luminosity  $L_X$ , are discussed in Sect. 3. The summary is given in Sect. 4. The database of X-ray detected Seyfert galaxies is quoted in the Appendix C. The X-ray light curves of variable Seyfert 1 galaxies are presented in Figs. C.1 to C.5 of the Appendix C.

## 2. ROSAT detected interacting and isolated Seyfert 1 & 2 galaxies

### 2.1. Identification procedure

For each source of the Rafanelli sample we have searched for X-ray detections within the *ROSAT* All-Sky Survey (RASS II catalogue; see Voges, Aschenbach, Boller et al., 1999 for references) and public PSPC<sup>1</sup> and HRI<sup>2</sup> pointed observations. The sources have been identified on X-ray contour maps overlaid to optical images taken from the Palomar Digitized Sky Survey (DSS). We have generated background subtracted contour maps for each selected *ROSAT* observation available for inspection as postscript files at <http://wave.xray.mpe.mpg.de/publications/papers/2001>. These files can also be retrieved via anonymous ftp from the address <ftp.xray.mpe.mpg.de><sup>3</sup>. Overlays with a dark background indicate pointed observations (HRI for HRI-data, without label for PSPC-data), whereas the grey background indicate *ROSAT* All-Sky survey data (PSPC). The quality of the identification of the X-ray source with the Seyfert galaxy is given in tables C.1 and C.2, 1 and 2 indicate high and low reliability of the identification, respectively.

### 2.2. Data reduction of survey and pointed observations

During the *ROSAT* All-Sky Survey the sources took from  $\sim 5$  s to  $\sim 30$  s to pass across the field of view of the PSPC detector on each orbit ( $\sim 96$  min). The difference in crossing time depends on the scan range over the field of view, which covers a circular area with a  $57'.3$  radius. We have only counted crossing times of individual sources through the PSPC detector, when the centroid source position was at least  $5'$  inside the detector. This prevents an underestimate of the source count rate due to the PSF. The resulting total exposure times, obtained taking the sum of crossing times of a source, are in the range of  $\sim 200$  s up to  $\sim 2000$  s spread over several days. For the *ROSAT* All-Sky Survey data reduction we have developed our own software modules, to take into account the requirements for data reduction of the survey scan mode.

The data analysis of pointed *ROSAT* PSPC and HRI observations was performed with the standard MIDAS/EXSAS software (Zimmermann et al. 1994). For this type of observation, the source is stationary centered

on the detector. The exposure times are in general significantly higher with respect to the survey observations (see tables C.3 and C.4 in Appendix C).

### 2.3. Spectral analysis

For each source with more than 60 photons detected in the All-Sky Survey and for all sources within PSPC-pointed observations we have performed a spectral analysis. A power-law model

$$f_E dE \propto E^{\Gamma+1} dE \quad (1)$$

fitted to the spectral data yields the power-law parameters; neutral absorbing hydrogen column density  $N_{\text{Hfit}}$ , photon index  $\Gamma$  and the monochromatic flux at 1 keV. The term  $f_E dE$  is the galaxy's energy flux between the photon energies  $E$  and  $E + dE$ . The soft X-ray flux in the energy range 0.1–2.4 keV, corrected for absorption by neutral hydrogen, was calculated using the spectral fit parameters. In the case of  $N_{\text{Hfit}} < N_{\text{Hgal}}$ , we have used the galactic absorption column density  $N_{\text{Hgal}}$  (Dickey & Lockman 1990).

For sources with  $\leq 60$  counts in the survey observations and for HRI observations we have converted the mean count rates to the flux using a power-law model with photon index fixed to  $\Gamma = -2.3$ , which is the typical value found for extragalactic objects with *ROSAT*, and the galactic hydrogen column density  $N_{\text{Hgal}}$ .

The soft X-ray flux was converted to luminosity using Eq. (7) of Schmidt & Green (1986):

$$L(E_1, E_2) = 4\pi \left(\frac{c}{H_0}\right)^2 C(z, \Gamma) A(z)^2 f(E_1, E_2) \quad (2)$$

where a power-law spectrum is assumed in the energy range  $(E_1, E_2)$ , so that the redshift-dependent functions  $C(z)$  and  $A(z)$  are given by:

$$C(z, \Gamma) = (1+z)^{\Gamma-2} \quad (3)$$

$$A(z) = 2[(1+z) - \sqrt{1+z}] \quad (4)$$

We adopted for the cosmological deceleration parameter  $q_0 = \frac{1}{2}$  and for the Hubble constant  $H_0 = 75 \text{ km s}^{-1} \text{ Mpc}^{-1}$ . The assumed photon index  $\Gamma$  is given in tables C.3 and C.4 and the redshift in tables C.1 and C.2.

### 2.4. Timing analysis

We have compared the survey and pointed count rates of individual sources in order to study the long-term variability (0.5 up to 8.0 years). For all pointed observations and for the All-Sky Survey data with more than 60 source counts we have produced the corresponding X-ray light curves (timescales up to a few days).

<sup>1</sup> Position Sensitive Proportional Counter

<sup>2</sup> High Resolution Imager

<sup>3</sup> subdirectory: publications/papers/2001/interacting-xray-seyferts

To produce the light curve of a survey source ( $\geq 60$  counts), we have defined a source cell with radius of  $5'$ . The background was determined from a source-free cell with a radius of  $5'$  located in the scan direction through the centroid position of the source. This was necessary, as the effective exposure time depends on the position of the scan direction and the background level may change for each time the path of source crosses the detector.

To take the *ROSAT* wobble for pointed observations into account we have used a minimum binsize of 400 s. From the light curve we have computed the mean count rate of the Seyfert 1 and Seyfert 2 galaxies, which are given in tables C.3 and C.4, respectively. The light curves of variable Seyfert 1 galaxies are given in Appendix C.

### 3. Results

In this section we present the X-ray properties of interacting and isolated Seyfert 1 & 2 galaxies. A description of the database is given in Subsect. 3.1. The spectral properties are listed in tables C.3 and C.4, respectively. The light curves for variable Seyfert 1 galaxies are shown in Figs. C.1 to C.5. The X-ray light curves of Seyfert 2 galaxies are given in Subsect. 3.3.2. Relations between  $\Gamma$ ,  $L_X$ , ( $L_{\text{fir}}$ ),  $Q$  and the Seyfert type are presented in Sect. 3.2. The correlation of the interaction strength  $Q$  and the X-ray luminosity  $L_X$  is described in Subsect. 3.2.2.

#### 3.1. The catalogue

We have detected 91 out of 99 Seyfert 1 and 47 out of 98 Seyfert 2 galaxies of the Rafanelli sample in the *ROSAT* X-ray band in pointed and/or All-Sky Survey observations. We have performed spectral analysis of the *ROSAT* PSPC observations for sources with more than 60 counts  $\text{s}^{-1}$ . The timing analysis has been performed for all sources. In this paper we only show light curves of sources with significant X-ray variability. Spectral information from the survey data could be obtained for 59 Seyfert 1 galaxies and only for one Seyfert 2 galaxy. The optical and X-ray properties of Seyfert 1 & 2 galaxies of this sample are listed in tables C.1 & C.2. The tables quote the name of the Seyfert galaxy (column 2), *ROSAT* name (column 3), redshift  $z$  (column 4), diameter of the Seyfert galaxy  $D_p$  (column 5), diameter of the companion galaxy  $D_c$  (column 6), separation between the components  $S$  (column 7), dimensionless gravitational interaction strength  $Q$  (column 8) (for description see Sect. 3.2.2) and the apparent visual magnitude  $V$  (column 9). The values of  $z$  and  $V$  are taken from Veron-Cetty & Veron catalogue (1991) and the units of  $D_p$ ,  $D_c$  and  $S$  are mm (POSS plates) with a scale  $\sim 13.4''/\text{mm}$  (Rafanelli et al., 1995). Columns 10 and 11 show the quality of the X-ray identifications both in the pointing and the survey observations, the identifications labeled either with 1 or 2, 1 and 2 indicating high and lower degree of reliability, respectively. In the last column we have listed

the classification of the Seyfert type (Sy1.0, Sy1.2, Sy1.5, Sy1.8, Sy1.9, Sy2.0) taken from the *Catalogue of Seyfert Galaxies* (Lipovetski et al., 1987). We have modified the Rafanelli et al. conventions ( $S1 = \text{Sy1.0} + \text{Sy1.2} + \text{Sy1.5}$  and  $S2 = \text{Sy1.8} + \text{Sy1.9} + \text{Sy2.0}$ ) to  $S1 = \text{Sy1.0} + \text{Sy1.2} + \text{Sy1.5} + \text{Sy1.8} + \text{Sy1.9}$  and  $S2 = \text{Sy2.0}$ . The classifications marked by a hash (#) indicate Narrow Line Seyfert 1 galaxies (NLS1) (e.g. Osterbrock & Pogge; Boller, Brandt & Fink 1996; Grupe 1996).

In Appendix C the X-ray properties obtained from the timing and spectral analysis are listed in tables C.3 and C.4. Columns 2 and 3 contain the *ROSAT* position. We mostly give the centroid source position from the pointed observation with the higher exposure times. The columns 4 and 5 list the count rates, columns 6 and 7 the corresponding exposure times, columns 8 and 9 the fluxes and columns 10 and 11 the luminosities of the sources detected in *ROSAT* pointing and survey observations, respectively. The survey count rates were taken from the RASS II catalogue and the pointing count rates were computed from the light curves of the sources. The apices  $p$  and  $h$  in column 4 indicate that the source data are taken from a PSPC or HRI observation. In the columns 8 and 9 we apply the apices  $f$  and  $c$  to mark the data produced by spectral fit or by count rates. This specification applies also for columns 10 and 11. The Galactic column density is given in column 12 (Dickey & Lockman, 1990), while the column density obtained from the spectral fit is given in column 13. The other spectral fit parameters, namely the monochromatic flux at 1keV and the photon index are also given in columns 14 and 15, respectively. The value  $\Gamma = -2.3$  was used, if no reliable spectral fit could be obtained. When spectral information was available from the survey as well as from the pointed data, we quote the results from the pointed observations.

In most cases for optically separated close pairs, we detected in the X-ray band an unresolved single source (see overlays<sup>4</sup>). The results of these spectral fits are listed in tables C.3 and C.4. When we detected two separate X-ray components, we created two spectra and we show the sum of the count rates, fluxes and luminosities and the single fit parameters ( $N_{\text{H}}$ ,  $f_{1\text{keV}}$ ,  $\Gamma$ ) of the Seyfert galaxy in the tables.

#### 3.2. Relations between $\Gamma$ , $L_X$ , $L_{\text{fir}}$ , $Q$ and Seyfert type

In this section we present the spectral properties of Seyfert 1 and Seyfert 2 galaxies in terms of the relations between the photon index  $\Gamma$ , the interaction strength  $Q$ , the X-ray luminosity  $L_X$ , the far-infrared luminosity  $L_{\text{fir}}$  and the Seyfert type.

<sup>4</sup> overlays are available at <http://wave.xray.mpe.mpg.de/publications/papers/2001>

### 3.2.1. Relations with $\Gamma$

In Fig. 1 we have correlated the photon index obtained from the power-law fit with the X-ray luminosity. Different subtypes of Seyfert 1 galaxies are marked with different labels. For low-luminosity Seyfert 1's, below about  $10^{42}$  erg s $^{-1}$ , where a significant contribution from the starburst is expected to contribute to the total luminosity, there is no clear trend between  $\Gamma_{\text{fit}}$  and  $L_X$ . However, for 'normal' Seyfert 1 type galaxies, a clear trend of a steepening of the X-ray spectrum with increasing X-ray luminosity is detected. A possible explanation for this effect might be a shifted and strengthened accretion disk spectrum in high-luminosity Seyferts. This is expected, as the high X-ray luminosity is most probably related to the accretion rate and/or the black hole mass (Frank, King, Raine, 1985). When fitting a simple-power law to the spectral data in the ROSAT energy band, steeper values for the photon index are expected to arise in the high luminosity Seyfert 1 galaxies. Another well-known effect is also present in Fig. 1, i.e. the steeper X-ray continua of NLS1s compared to broad-line Seyfert 1 galaxies (Boller, Brandt & Fink 1996).

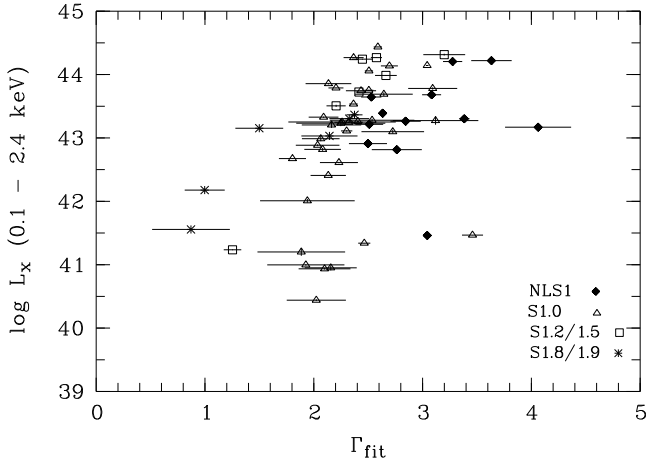


**Fig. 1.** Relation between the X-ray luminosity  $L_X$  [erg s $^{-1}$ ] and the photon index for Seyfert 1 galaxies. The different subtypes of Seyfert 1 galaxies (NLS1s, Seyfert 1.x) are plotted with different symbols. For Seyfert 1 galaxies above a X-ray luminosity of about  $10^{42}$  erg s $^{-1}$  we find a strong trend of an increasing photon index with increasing X-ray luminosity.

For Seyfert 2 galaxies, we found no significant trend for an increasing photon index with increasing X-ray luminosity. Higher sensitivity measurements, e.g. with XMM-Newton, are necessary to search for a correlation between the photon index and the X-ray luminosity for Seyfert 2 galaxies.

In Fig. 2 we show the distribution of photon indices, obtained from the spectral fits, versus the Seyfert type (we have plotted NLS1s at an x-axis value of 0.9). Only Seyfert galaxies with errors in the photon index smaller than 0.5

have been included. As expected, NLS1s show the largest values of the photon index, compared to Seyfert 1 galaxies. Seyfert 2 galaxies show similar steep X-ray continua compared to NLS1s. The Seyfert 1 galaxies show similar values of the photon indices as given by Walter & Fink (1993).

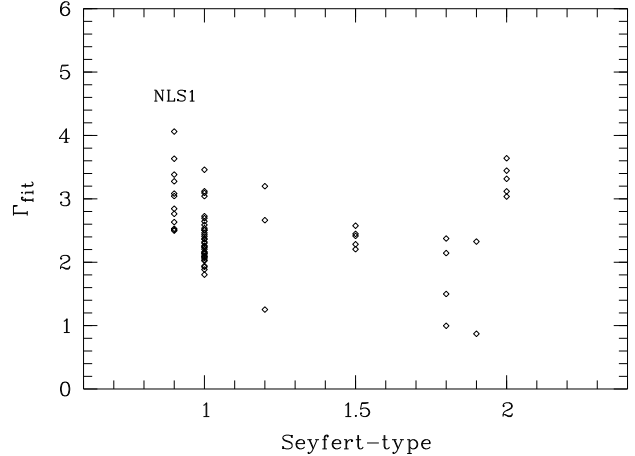


**Fig. 2.** Distribution of photon indices, obtained from the spectral fits, versus the Seyfert type (we have plotted NLS1s at an x-axis value of 0.9). The highest values in the photon indices are found for NLS1s and for Seyfert 2 galaxies.

### 3.2.2. Interaction strength $Q$ - luminosity $L_X$ , $L_{\text{fir}}$ relations

In order to derive the interaction strength  $Q$  we concentrate on the tidal force per unit mass produced by a companion on a primary galaxy, which is proportional to  $M_c \cdot R^{-3}$ .  $M_c$  is the mass of the companion and  $R$  is its distance from the center of the primary galaxy. In most cases,  $M_c$  and the absolute value of  $R$  are unknown. Instead, these parameters are related to the dimensions of the pair. Rubin et al. (1982) describe the dependence of the mass  $M$  of a galaxy on the size of its major axis  $d$  as  $M \propto d^\gamma$  and we use  $\gamma = 1.5$  (Dahari, 1984). If we use the apparent diameter of the primary galaxy  $D_p$  as a scaling factor, we obtain:

$$M_c \propto (D_c/D_p)^{1.5} \quad \text{and} \quad R \propto S/D_p \quad (5)$$

Using these relations we get as dimensionless gravitational interaction strength  $Q$ :

$$\frac{M_c}{R^3} \propto \frac{(D_c \cdot D_p)^{1.5}}{S^3} \equiv Q \quad (6)$$

This parameter is obviously large for close and relatively large companions.

Fig. 3 shows the interaction strength  $Q$  vs. the far-infrared luminosity  $L_{\text{fir}}$  for Seyfert 1 galaxies. For Seyfert

1 galaxies, the far-infrared luminosity increases with interaction strength. The low-luminosity Seyfert 1 galaxies NGC 5273, NGC 4278, NGC 3227, (NGC 4258 is not detected in the IRAS Faint Source Catalogue) also show the trend of increasing X-ray and far-infrared luminosity with interaction strength  $Q$ . We speculate a large interaction strength of  $Q = 15.1 \pm 4.4$  for the galaxy Mkn 1040 causes the relatively high X-ray (see fig. 4) and far-infrared luminosity and that the galaxy belongs to the low-luminosity population discussed above. To test the correlation we have calculated the linear-correlation coefficient  $r$  and the probability  $P(r, N)$  for a linear correlation. For the high-luminosity objects we obtain  $r = 0.3271$  and  $P(r, 22) \approx 85\%$  ( $\sim 1.5\sigma$ ), whereas we got for the low-luminosity Seyferts  $r = 0.8478$  and  $P(r, 4) \approx 85\%$  ( $\sim 1.5\sigma$ ).

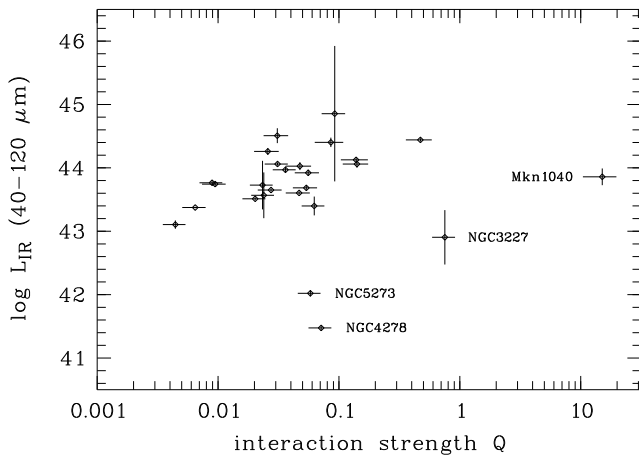


**Fig. 3.** Dimensionless gravitational interaction strength  $Q$  vs. far-infrared luminosity  $L_{\text{fir}}$  [ $\text{erg s}^{-1}$ ] for Seyfert 1.x galaxies. The plot suggests an increase in luminosity for increasing values of the interaction strength.

Fig. 4 shows the interaction strength  $Q$  vs. the soft X-ray luminosity  $L_X$  for Seyfert 1 galaxies. For Seyfert 1 galaxies with  $L_X > 10^{42}$  there is a tendency for a luminosity increase with increasing interaction strength. The labelled sources refer to the low-luminosity Seyfert 1 galaxies in our sample. As discussed for the relation between the far-infrared luminosity and the interaction strength  $Q$ , both the low-luminosity Seyfert 1's and the high-luminosity Seyfert 1's increase in X-ray luminosity when the interaction strength  $Q$  is increased. The high spread of the distribution is quite likely produced by an overlap of effects from starburst and AGN. In the case of infrared luminosity (fig. 3) only the starburst play a role. The linear-correlation test resulted in  $r = 0.2880$  and  $P(r, 27) \approx 85\%$  ( $\sim 1.5\sigma$ ) for the high-luminosity Seyferts and in  $r = 0.8233$  and  $P(r, 5) \approx 92\%$  ( $\sim 1.7\sigma$ ) for the low-luminosity objects.

The data points in Fig. 4 also include ROSAT pointed observations and Seyfert 1.8 and 1.9 galaxies, which complete the relation between  $L_X$  and  $Q$  first discussed by Rafanelli et al. (1997). For Seyfert 2 galaxies we found

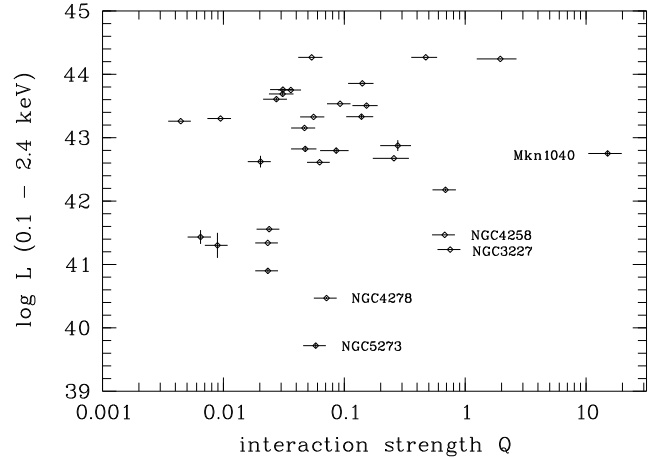


**Fig. 4.** Dimensionless gravitational interaction strength  $Q$  vs. soft X-ray luminosity  $L_X$  [ $\text{erg s}^{-1}$ ] for Seyfert 1.x galaxies. The plot suggests an increase in luminosity for increasing values of the interaction strength. The marked objects with low luminosities are probably absorbed sources with emission from the circumnuclear starbursts and scattered radiation from the nuclei.

no correlation between the soft X-ray luminosity and the interaction strength. In Sect. 4 we discuss the problems in determining precisely the X-ray properties of obscured Seyfert 2 galaxies.

### 3.2.3. Far-infrared relations

In order to estimate the starburst activity we have investigated the far-infrared luminosity  $L_{\text{fir}}$  using the far-infrared fluxes  $f_{\text{fir}}$  at 60 and 100  $\mu\text{m}$  from the IRAS Faint Source Catalogue. The total far-infrared fluxes  $f_{\text{fir}}$  (40 – 120  $\mu\text{m}$ ) were computed following Helou (1985) from the IRAS 60  $\mu\text{m}$  and 100  $\mu\text{m}$  band fluxes:

$$f_{\text{fir}} = 1.26 \cdot 10^{-11} (2.58 f_{60} + f_{100}) \text{ erg cm}^{-2} \text{ s}^{-1} \quad (7)$$

where  $f_{60}$  and  $f_{100}$  are given in Jansky. The far-infrared fluxes were converted to luminosities using Eq. 2 in Sect. 2.3. For the photon index we assumed  $\Gamma = 1.5$ .

The ratio between far-infrared and soft X-ray luminosity  $L_X/L_{\text{fir}}$  and its dependence on the far-infrared luminosity  $L_{\text{fir}}$  is shown in fig. 5 for all Seyfert types. Interestingly, NLS1 galaxies show a similar distribution of the far-infrared luminosity as the Seyfert 2 galaxies. The far-infrared luminosity distribution is significantly different for Seyfert 1 galaxies compared to NLS1 and Seyfert 2's.

In fig. 6 we plot the ratio  $L_X/L_{\text{fir}}$  vs. the interaction strength  $Q$  for all Seyfert types. For Seyfert 1 galaxies no correlation between the luminosity ratio and the interaction strength is found. If we can interpret the far-infrared luminosity as mainly caused by starburst activity, and the X-ray luminosity as mainly caused by accretion processes, this indicates that starburst and AGN activity increase proportionally.

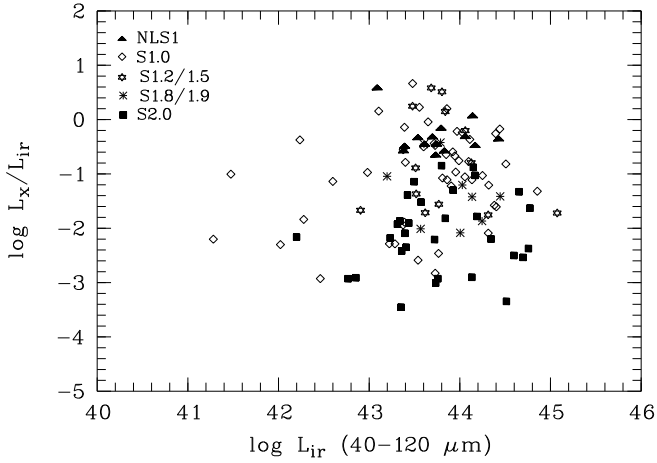


**Fig. 5.** Soft X-ray to far-infrared ( $40–120\mu\text{m}$ ) luminosity ratio  $L_X/L_{\text{fir}}$  vs. far-infrared luminosity  $L_{\text{fir}}$  [ $\text{erg s}^{-1}$ ] for all types of Seyfert galaxies.

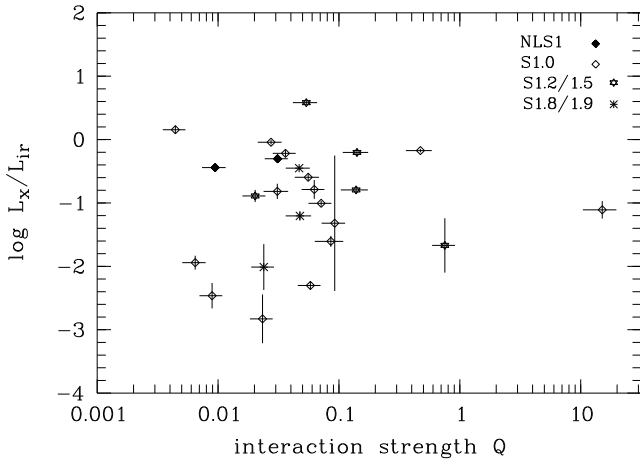


**Fig. 6.** Soft X-ray to far-infrared ( $40–120\mu\text{m}$ ) luminosity ratio  $L_X/L_{\text{fir}}$  vs. dimensionless gravitational interaction strength  $Q$  for all types of Seyfert 1.x galaxies. There is no correlation noticeable.

The interpretations of the results are discussed in Sect. 4.

### 3.3. Timing properties

Below we discuss the long-term (time scales between half a year up to 8 years) X-ray and short-term (time scales of order up to a few days) variability of interacting and isolated Seyfert 1 and 2 galaxies.

#### 3.3.1. X-ray variable Seyfert 1 galaxies

In our sample 59% of the X-ray detected Seyfert 1 galaxies show significant X-ray variability during the ROSAT All-Sky Survey and ROSAT pointed observations. The corresponding X-ray light curves are shown in Appendix C.

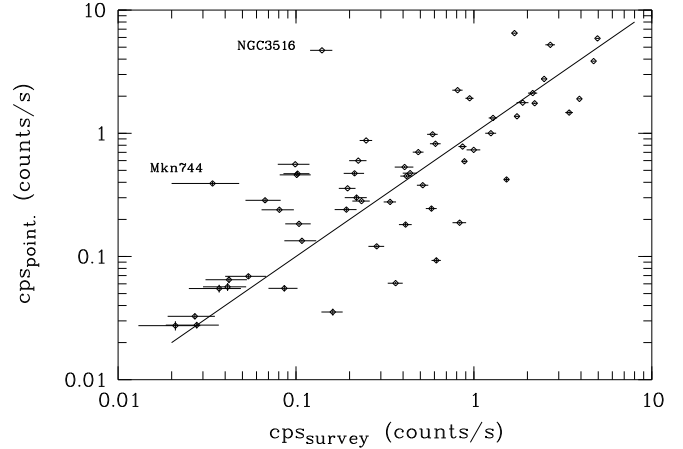


**Fig. 7.** Long-term variability of interacting and isolated Seyfert 1 galaxies. The most extreme factor of amplitude variability of about 33 is found for NGC 3516.

In fig. 7 we compare the ROSAT All-Sky Survey count rate with the count rate measured in ROSAT PSPC pointed observations. The most extreme factor of variability is found for NGC 3516 (a factor of about 33 on a timescale of 718 days).

#### 3.3.2. The X-ray light curves for Seyfert 2 galaxies

For interacting and isolated Seyfert 2 galaxies no indication for significant X-ray variability on timescales above 0.5 years is found by comparing the ROSAT All-Sky Survey and ROSAT PSPC pointed observations (Fig. 8). The galaxy NGC 5506 is classified by Lipovetski et al. (1987) as Seyfert type 2. This source exhibits the largest factor of variability of about 2.7 on a timescale of 375 days.

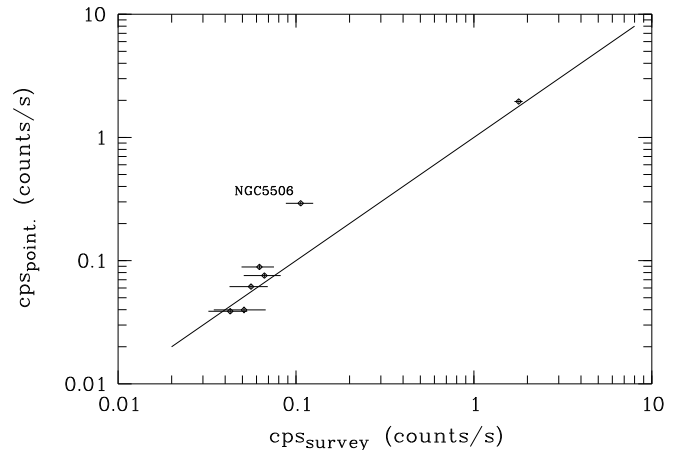


**Fig. 8.** The long-term variability of interacting and isolated Seyfert 2 galaxies.

However, for three out of the 36 Seyfert 2 galaxies, NGC 1068, NGC 4388 and IRAS F01475-0740, indications

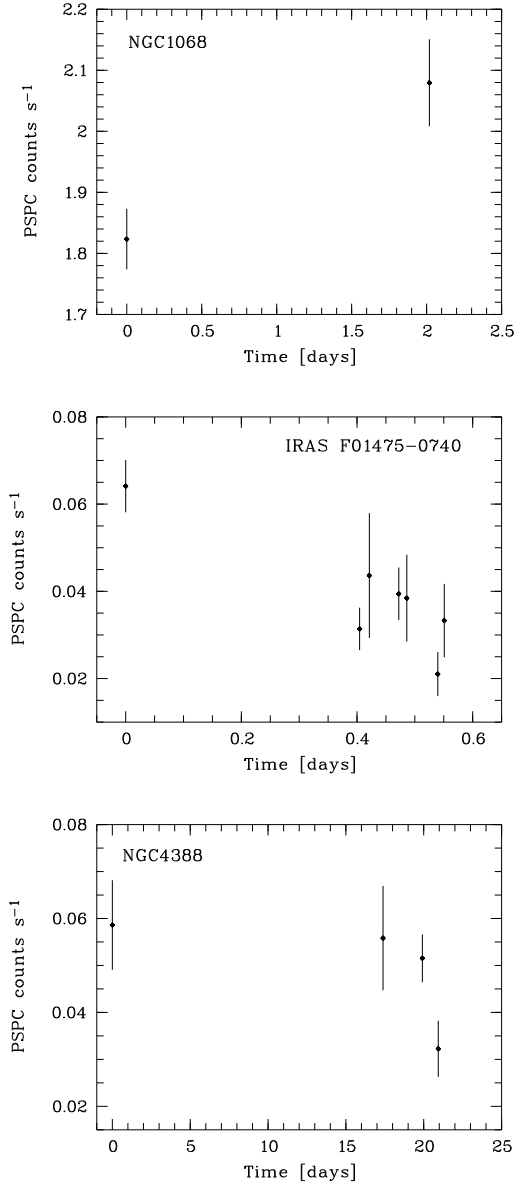


**Fig. 9.** PSpC pointed light curves of the Seyfert 2.0 galaxies NGC 1068 (*top*) with the probabilities of variability of 99.83% ( $3\sigma$ ), IRAS 0147-0740 (*middle*) with 99.9989% ( $4\sigma$ ) and NGC 4388 (*bottom*) with 97.896% ( $2\sigma$ ).

for X-ray variability are found in ROSAT pointed observations. In fig.9 (*top*) the pointed observation light curve of the Seyfert 2 galaxy NGC 1068 is shown. An increase in count rate from 1.823 to 2.080 counts  $s^{-1}$ , corresponding to a factor of 1.14 or  $\Delta cps = 0.256$ , within 2 days is detected. A constant model fit using the  $\chi^2$  test can be rejected with a probability of 99.83%, corresponding to  $3\sigma$ . Indications for X-ray variability in NGC 1068 are also found in other ROSAT pointed observations (cf. fig. B.1). The ROSAT PSpC light curve for the Seyfert 2 galaxy IRAS 01475-0748 is shown in fig. 9 (*middle*). A decrease in the count rate from 0.064 to 0.021 counts  $s^{-1}$  within 12.9 hours is detected. This variability corresponds to a factor of 3 and to a change in the count rate of  $\Delta cps = 0.043$ . A constant model fit gives a probability of 99.9989% ( $4\sigma$ ). In

fig. 9 (*bottom*) the X-ray light curve of NGC 4388 is shown. The count rate decreases from 0.0586 to 0.0322 counts  $s^{-1}$  corresponding to a factor of variability of about 1.8 and a change in the count rate of  $\Delta cps = 0.026$  within 21 days. A constant model fit can be rejected with a probability of 97.896%, corresponding to  $2\sigma$ .

Recently, Georgantopoulos & Papadakis (2000) found evidence for spectral (and timing) variability for four Seyfert 2 galaxies in RXTE observations.

#### 4. Discussion and summary

We have detected 92% of interacting or isolated Seyfert 1 and 48% of Seyfert 2 galaxies in the optically selected sample of Rafanelli et al. (1995). The soft X-ray spectral and timing properties are presented in tables C.3 & C.4 (note the different combination of Seyfert types; 102 S1.x and 36 S2).

For Seyfert 1 galaxies we have found a correlation between photon index  $\Gamma$  and the soft X-ray luminosity  $L_X$ . A clear trend of a steepening of the X-ray spectrum with increasing X-ray luminosity is detected. High X-ray luminosity is most probably related to the accretion rate and/or the black hole mass. Therefore, a possible explanation for this effect might be a shifted and strengthened accretion disk spectrum in high-luminosity Seyferts. We confirm that NLS1s have steeper X-ray continua than broad-line Seyfert 1 galaxies. Seyfert 2 galaxies show similar steep X-ray continua compared to NLS1s. While the steep X-ray continua for NLS1s are expected to be related with high values for the Eddington luminosity in combination with small black hole masses, the steep X-ray continua for Seyfert 2 galaxies are probably due to the dominant X-ray line emission from the circumnuclear starburst.

Our data result in an increasing far-infrared and increasing X-ray luminosity with increasing interaction strength for Seyfert 1 galaxies. Both strengthen the suggestion that galaxy interaction triggers an increased accretion rate and starburst rate. NLS1s and Seyfert 2 galaxies show the highest values of far-infrared luminosity compared to Seyfert 1 galaxies. This fact points to nuclear starburst activity taking place in NLS1 galaxies as suggested by Mathur (2000).

For Seyfert 2 galaxies, we found no significant correlations between the X-ray luminosity and photon index or interaction strength. The main reason is the lack of penetration through the high column densities in Seyfert 2 galaxies with soft X-rays. The ROSAT  $N_H$  values derived from the spectral fitting are therefore lower limits to the true absorbing columns in Seyfert 2 galaxies. This is supported by comparing our results with those from higher energy satellites. Bassani et al. (1999) investigated the hard X-ray spectra of a large sample of Seyfert 2 galaxies with *Ginga*, *ASCA* and *BeppoSAX*. The authors found a large population of strong-absorbed objects with column densities  $N_H \geq 10^{23} \text{cm}^{-2}$ , including many Compton-thick candidates. The column densities obtained

from the soft X-ray spectra show significantly lower values for many sources. The reason for this is the different origin of the hard and soft X-ray radiation. The column densities are likely able to determine the outer regions of the molecular torus at soft X-rays, because the radiation penetrates less absorbing material. Only the hard X-ray radiation above a few keV is able to pass interior regions of the torus and leads to higher column densities. Therefore, our results for Seyfert 2 galaxies are only a lower limit to the intrinsic column density. The fluxes and luminosities of Seyfert 2 galaxies given in table C.4 are considered as lower limits to the intrinsic values. Finally, the soft X-ray emission of Seyfert 2 galaxies is probably due to emission from the circumnuclear starburst together with radiation from the nuclei, scattered and reflected by the molecular torus. Moreover, we found no correlation between the far-infrared luminosity and interaction strength for the Seyfert 2 sample.

Higher sensitivity observations with *XMM-Newton* and *Chandra* are expected to confirm the short-time variability of the three Seyfert 2 galaxies.

We have investigated the variability of Seyfert 1 and 2 galaxies on short and long timescales and found indications for variability in three Seyfert 2.0 galaxies on short timescales (NGC 1068, IRAS 0147-0740, NGC 4388). A possible explanation for this variability might be the presence of boreholes in the absorbing molecular torus around the central black hole region. Significant X-ray variability during the *ROSAT* pointed and survey observations were detected for 58 percent of the Seyfert 1 galaxies.

*Acknowledgements.* We thank Prof. Joachim Trümper for comments and A. Vogler for help in producing the images with overlaid X-ray contours. We are grateful to Dr. W. Voges for his help in the catalogue preparation. The *ROSAT* project is supported by the Bundesministerium für Bildung und Forschung (BMBF/DLR) and by the Max-Planck Society (MPG).

This paper can be retrieved via WWW from our pre-print server: <http://www.xray.mpe.mpg.de/~pfefferk/>

## References

- Barnes J.E. & Hernquist L.E., *ApJ* **370** (1991) L65  
 Barnes J.E. & Hernquist L., *ApJ* **471** (1996) 115B  
 Bassani L., Dadina M., Maiolino R. & Salvati M. et al, *ApJS* **121** (1999) 473  
 Bernlöhr K., *A&A* **268** (1993) 25  
 Boller Th., Brandt W.N. & Fink H., *A&A* **305** (1996) 53  
 Bushouse H.A., *ApJ* **320** (1987) 49  
 Dahari O., *AJ* **89** (1984) 966  
 Dickey J.M. & Lockman, F.J., *ARA&A* **28** (1990) 215  
 Frank J., King A.R., Raine D.J., *Accretion power in astrophysics* (Cambridge University Press) (1985) 90  
 Freedman W.L. et al, *ApJ* **427** (1994) 628  
 Grupe D., *Properties of bright soft X-ray selected ROSAT AGN* (1996), (dissertation submitted Georg-August university, Göttingen, Germany)  
 Georgantopoulos I., Papadakis I.E., *MNRAS submitted astro-ph/0008295* (2000)  
 Hummel E., *A&A* **96** (1981) 111  
 Helou G., Soifer B.T., Rowan-Robinson M., *ApJ* **298** (1985) L7  
 Jog C.J. & Das M., *ApJ* **400** (1992) 476  
 Jog C.J. & Solomon P.M., *ApJ* **387** (1992) 152  
 Kennicutt Jr. R.C., Keel W.C., van der Hulst J.M., Hummel E. & Roettiger K.A. *AJ* **93** (1987) 1011  
 Lipovetski V.A., Neizvestny S.J. & Neizvestnaya O.M. *A Catalogue of Seyfert Galaxies* (1987), (Communications of the Special Astrophysical Observatory), p. 55  
 Mathur S., *MNRAS* **314** (2000) L17  
 Mihos J.C. & Hernquist L., *ApJ* **464** (1996) 641  
 Osterbrock D.E. & Pogge R.W., *ApJ* **297** (1985) 166  
 Pietsch W., Trinchieri G., Arp H. & Sulentic J. W., *A&A* **322** (1997) 89P  
 Rafanelli P., Violato M. & Baruffolo A., *AJ* **109** (1995) 1546  
 Rafanelli P., Piro L., Radovich M. et. al, *Memorie della Societa Astronomia Italiana* **68** (1997) 301  
 Rafanelli, P., Osterbrock, D. E., Pogge, R. W., *AJ* **99** (1990) 53R  
 Rubin V.C., Ford Jr. W.K., Thonnard N. & Burstein D., *ApJ* **261** (1982) 439  
 Schmidt M. & Green R.F., *ApJ* **305** (1986) 68  
 Smith E.P. & Kassim N.E., *AJ* **105** (1993) 46  
 Tesco C.M., Dressel L.L. & Wolstencroft R.D., *ApJ* **414** (1993) 120  
 Veron-Cetty M.P. & Veron P., *A Catalogue of Quasars and Active Nuclei*, (1991), 5th ed. (ESO, Garching near Munich)  
 Voges W., Aschenbach B., Boller Th., et al. *A&A* **349** (1999) 389  
 Walter R. & Fink H.H., *A&A* **274** (1993) 105W  
 Zimmermann H.U., Belloni T., Izzo C., Kahabka P. & Schwentker O., *MPE Report 257* (1994)

## Appendix A: Notes on individual sources

- **NGC 2992:** In the case of NGC 2992 and its companion we detect two spatially separated X-ray components. In table C.4 of Appendix C we give the sum of the count rates, fluxes and luminosities for this system. For the completion of the database we add here the individual values of the source and the companion. The spectrum of NGC2992 shows a high absorption and a low photon index with an integrated flux of  $2.815 \cdot 10^{-12}$  erg cm<sup>-2</sup> s<sup>-1</sup> corresponding to a luminosity of  $2.616 \cdot 10^{41}$  erg s<sup>-1</sup>. The spectrum of the companion results in a flux of  $1.061 \cdot 10^{-12}$  erg cm<sup>-2</sup> s<sup>-1</sup> corresponding to a luminosity of  $9.987 \cdot 10^{40}$  erg s<sup>-1</sup>. The spectral fit parameters for the companion are  $N_{\text{Hfit}} = 0.854 \cdot 10^{21}$  cm<sup>-2</sup> and  $\Gamma = -2.72$ . NGC 2992 is classified by Lipovetski et al. (1987) as a Seyfert 1.9 galaxy and we found a variability of this object over short and long timescales (see Sect. 3.3.2).
- **NGC 5506:** The soft X-ray spectrum of the Seyfert galaxy NGC 5506 is highly absorbed and no reliable spectral fit parameters can be obtained. Thus, we have used for  $N_{\text{H}} = 1.0 \cdot 10^{21}$  cm<sup>-2</sup> as a lower limit in table C.4.



- **NGC 5953:** This interacting system (Rafanelli, Osterbrock, Pogge; 1990) is detected in the survey and pointed observations. The X-ray emission of this system in the pointed observation is mainly caused by the Seyfert 2 galaxy NGC 5953. In the survey observation the emission is centered on the companion of NGC 5953 and no emission from the Seyfert 2 galaxy is detected. Due to the PSPC pointing accuracy we are not able to decide whether NGC 5953 is a transient source in the soft X-ray band.
- **Mkn 684:** For Mkn 684 we assume the classification as a NLS1 galaxy by Osterbrock & Pogge (1985) and Grupe (1996).
- **NGC 7319,** a member of the Stefan’s Quintet group, is detected with the PSPC (pointed and survey) and HRI detector by *ROSAT*. The PSPC survey and pointed observations showed unresolved X-ray emission from the group and the intergalactic gas (Pietsch W. & Trinchieri G., 1997). The HRI pointed observation as used to determine the flux of the Seyfert 2 galaxy.
- **NGC 3031:** For NGC 3031 (M81) we used the distance of 3.63 Mpc given in Freedman et al. (1994) to compute the luminosity of this object ( $z < 0$ ).

## Appendix B: Light curves of NGC 1068

In Fig. B.1 we give the remaining PSPC and HRI light curves of the Seyfert 2 galaxy NGC 1068.

## Appendix C: The Catalogue - data tables and light curves

In this section we show the results of our studies of the X-ray properties of the Seyfert 1 and 2 galaxies in tables C.3 & C.4, while in tables C.1 & C.2, general and optical properties are listed. The light curves of variable Seyfert 1 galaxies are also summarized in this appendix in Figs. C.1 to C.5. To distinguish the survey from the pointing light curves we have labeled the survey curves. The pointed light curves are distinguished by the y-axis in PSPC or HRI based data.

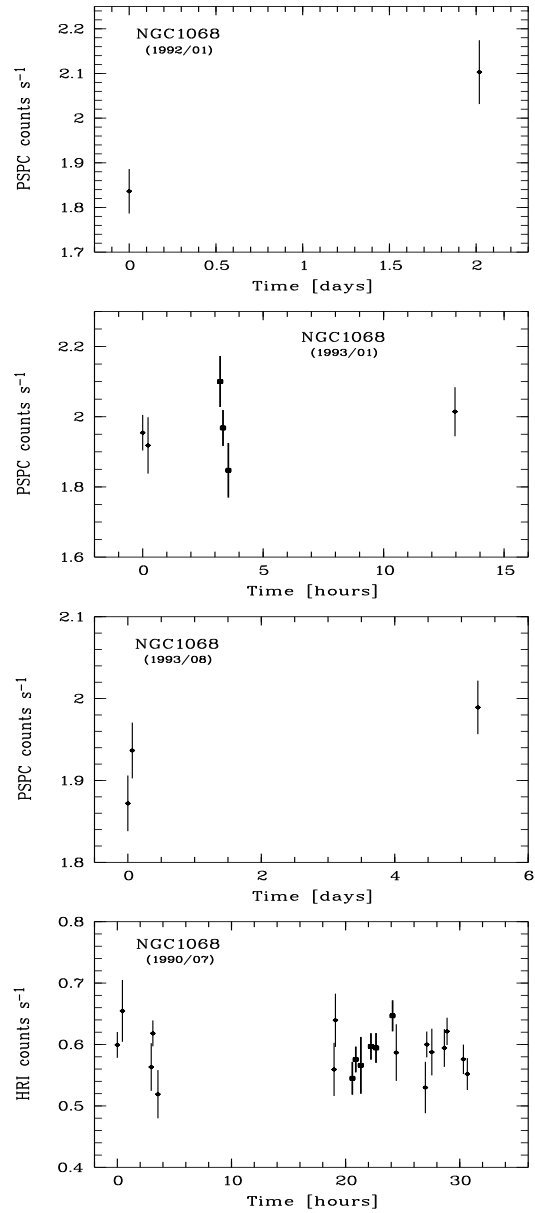


**Fig. B.1.** Pointing light curves of the Seyfert 2.0 galaxies NGC 1068 (from top to bottom): *first panel:* this PSPC light curve of NGC1068 from 1992/01 was described in Sect. 3.3.2 already. *second panel:* The bold data points in the light curve of the PSPC observation from 1993/01 indicate a variability with a probability of 94.24% ( $\sim 2\sigma$ ). The count rate decrease from 2.10 to 1.85 counts  $s^{-1}$  corresponds to a factor of 1.14 or  $\Delta_{cps} = 0.253$  within 1 hour. *third panel:* The third PSPC pointing light curve of NGC 1068 shows a probability of variability of 95.47% ( $2\sigma$ ) with an increase of  $\Delta_{cps} = 0.117$  counts  $s^{-1}$ . *fourth panel:* A HRI pointed light curve of this object indicates also a variability, with a probability of 88,82% for the bold data points. The count rate increase from 0.545 to 0.647 counts  $s^{-1}$  within 3.5 hours correlates with a variability factor of 1.19 or  $\Delta_{cps} = 0.102$ .

**Table C.1. Seyfert1 galaxies:** A part of the Rafanelli sample of interacting or isolated Seyfert 1 galaxies detected by *ROSAT*. The table contains optical and generical properties as well as some results from the investigations of the Rafanelli group (Rafanelli et al., 1995). Col(2) - object name, col(3) - ROSAT name, col(4) - redshift, col(5&6) - diameter of Seyfert galaxy and companion, col(7) - distance between the components, col(8) - interaction strength, col(9) - apparent visual magnitude, col(10&11) - quality of X-ray identification (1: high, 2: lower degree of reliability) and col(12) - Seyfert type. The upper index # in col(12) marks objects, which are classified as NLS1 galaxy (D.E. Osterbrock & R.W. Pogge (1985); Th. Boller, W.N.Brandt & H.Fink 1996; D.Grupe 1996).

Nr.	name	ROSAT name	z	$D_p$ mm	$D_c$ mm	S mm	Q	V mag	id point.	sur.	Sy type
1	Mkn334	1RXS J000308.6+215728	0.022	3.7	-	-	-	14.62	-	1	1.8
2	Mkn335	1RXP J000619.2+201224	0.025	1.2	-	-	-	13.85	1	1	1.0
3	Mkn1146	1RXS J004719.4+144215	0.039	2.6	-	-	-	15.28	-	1	1.0
4	Mkn352	1RXP J005953.3+314947	0.015	1.4	-	-	-	14.66	1	1	1.0
5	Mkn1152	1RXP J011350.1-145034	0.052	2.2	1.2	1.3	1.9524±0.7060	15.00	1	1	1.5
6	Mkn993	1RXS J012531.4+320800	0.017	7.5	-	-	-	13.96	-	1	1.9
7	Mkn975	1RXS J011350.4+131534	0.050	2.0	-	-	-	14.50	-	1	1.5
8	Mkn358	1RXS J012634.2+313659	0.042	2.8	-	-	-	15.23	-	1	1.0
9	Mkn359	1RXP J012732.8+191051	0.017	2.6	-	-	-	14.21	1	1	1.5 <sup>#</sup>
10	Mkn1018	1RXP J020616.0-001732	0.043	2.6	-	-	-	14.65	1	1	1.9
11	Mkn590	1RXP J021433.7-004604	0.027	4.1	0.8	4.8	0.0537±0.0122	13.55	1	1	1.5
12	Mkn1040	1RXS J022814.6+311838	0.016	9.8	1.8	1.7	15.0800±4.6514	14.74	-	1	1.0
13	Mkn1044	1RXP J023005.8-085940	0.016	1.7	-	-	-	14.67	1	1	1.0 <sup>#</sup>
14	NGC985	1RXP J023437.9-084709	0.043	3.2	-	-	-	14.95	1	1	1.0
15	Mkn595	1RXS J024135.2+071117	0.028	1.7	1.0	2.0	0.2771±0.0790	14.40	-	1	1.0
16	Mkn372	1RXP J024920.6+191822	0.031	1.7	-	-	-	14.81	1	1	1.8
17	Mkn609	1RXP J032525.5-060827	0.032	1.1	-	-	-	14.12	1	1	1.8
18	Mkn618	1RXS J043622.3-102226	0.035	2.6	0.7	4.3	0.0309±0.0071	14.65	1	1	1.0
19	Mkn6	1RXS J065209.8+742537	0.019	1.8	-	-	-	14.02	-	1	1.5
20	Mkn374	1RXS J065938.5+541136	0.044	1.6	-	-	-	14.38	-	2	1.2
21	Mkn9	1RXS J073657.0+584610	0.039	1.7	-	-	-	14.68	-	1	1.0
22	Mkn79	1RXP J074233.5+494838	0.022	3.3	-	-	-	14.78	1	1	1.2
23	Mkn10	1RXP J074728.6+605552	0.030	5.2	2.1	10.0	0.0361±0.0078	14.70	1	1	1.0
24	Mkn382	1RXS J075526.1+391111	0.034	2.1	-	-	-	15.50	1	1	1.0
25	Mkn1218	1RXP J083810.8+245336	0.028	2.6	1.3	5.1	0.0468±0.0105	14.12	1	1	1.8
26	NGC2639	1RXP J084338.0+501207	0.011	6.5	-	-	-	11.39	1	-	1.0
27	NGC2782	1RXH J091405.1+400651	0.008	8.5	1.5	12.5	0.0233±0.0050	13.45	1	-	1.0
28	Mkn704	1RXS J091826.2+161825	0.029	2.5	1.1	5.5	0.0274±0.0061	14.12	-	1	1.0
29	Mkn110	1RXP J092512.8+521712	0.036	1.2	-	-	-	15.37	1	1	1.0
30	Mkn705	1RXP J092603.0+124359	0.028	2.1	-	-	-	14.55	1	1	1.0 <sup>#</sup>
31	NGC2992	1RXP J094541.6-141938	0.007	5.6	2.7	13.5	0.0239±0.0051	13.78	1	1	1.9
32	Mkn124	1RXS J094841.6+502926	0.056	1.0	-	-	-	15.33	-	1	1.0
33	Mkn1239	1RXP J095219.0-013631	0.019	1.3	-	-	-	14.33	1	1	1.5 <sup>#</sup>
34	NGC3031	1RXP J095532.8+690354	0.000	6.9	-	-	-	11.72	1	1	1.5
35	NGC3080	1RXP J095956.3+130242	0.035	2.2	-	-	-	15.01	1	1	1.0
36	NGC3185	1RXP J101737.8+214124	0.004	0.7	-	-	-	12.73	1	-	1.0
37	Mkn141	1RXS J101912.1+635802	0.039	1.5	1.4	2.8	0.1386±0.0349	15.27	1	1	1.2
38	NGC3227	1RXP J102330.2+195150	0.003	12.5	8.0	11.0	0.7513±0.1615	11.29	1	1	1.0
39	Mkn142	1RXP J102532.5+514045	0.045	1.0	-	-	-	15.50	1	1	1.0 <sup>#</sup>
40	Mkn634	1RXS J105801.2+202937	0.066	1.8	-	-	-	15.49	-	2	1.0
41	NGC3516	1RXP J110649.0+723406	0.009	7.0	1.7	21.0	0.0044±0.0009	12.23	1	1	1.0
42	Mkn732	1RXS J111349.5+093518	0.030	2.6	-	-	-	14.00	-	1	1.0
43	Mkn734	1RXP J112146.9+114418	0.049	1.1	-	-	-	14.71	1	1	1.0 <sup>#</sup>
44	Mkn40	1RXP J112536.6+542303	0.020	1.3	0.7	1.5	0.2572±0.0851	15.39	1	2	1.0
45	Mkn739A	1RXP J113629.2+213543	0.030	1.8	-	-	-	14.02	1	1	1.0
46	Mkn744	1RXP J113942.8+315439	0.010	4.8	7.5	6.8	0.6870±0.1507	13.74	1	1	1.8
47	NGC3884	1RXS J114611.5+202355	0.023	6.7	-	-	-	12.40	-	1	1.0
48	Mkn42	1RXP J115341.7+461254	0.024	2.1	-	-	-	15.45	1	1	1.0 <sup>#</sup>
49	Mkn1310	1RXP J120114.9-034031	0.019	1.2	-	-	-	15.08	1	1	1.0
50	NGC4051	1RXP J120310.2+443156	0.002	19.0	-	-	-	12.12	1	1	1.0 <sup>#</sup>
51	NGC4151	1RXP J121032.4+392418	0.003	12.5	3.6	23.5	0.0233±0.0049	11.26	1	1	1.0
52	Mkn1469	1RXS J121607.4+504926	0.031	1.9	-	-	-	14.20	-	1	1.5
53	NGC4235	1RXP J121710.1+071135	0.007	5.1	-	-	-	13.50	1	1	1.0
54	Mkn766	1RXP J121826.4+294847	0.012	3.0	-	-	-	13.00	1	1	1.0 <sup>#</sup>
55	NGC4258	1RXP J121856.4+471755	0.002	37.0	3.0	12.0	0.6768±0.1452	11.30	1	1	1.0
56	NGC4278	1RXP J122007.2+291646	0.002	7.5	3.3	12.0	0.0713±0.0153	10.51	1	1	1.0
57	Mkn205	1RXP J122144.5+751840	0.070	1.1	6.0	3.3	0.4718±0.1139	15.24	1	1	1.0
58	Mkn50	1RXS J122324.4+024040	0.023	1.0	-	-	-	15.17	-	2	1.0
59	NGC4593	1RXP J123939.2-052046	0.009	17.0	3.0	18.0	0.0625±0.0133	13.19	1	1	1.0
60	NGC4594	1RXP J123959.2-113731	0.002	33.0	-	-	-	9.64	1	1	1.0
61	NGC4639	1RXP J124252.2+131527	0.001	6.0	-	-	-	11.00	1	1	1.0
62	IR1249-1308	1RXS J125212.5-132450	0.014	2.7	-	-	-	14.47	-	1	1.0 <sup>#</sup>
63	Mkn236	1RXS J130021.2+613919	0.052	1.5	-	-	-	15.45	-	1	1.0
64	Mkn783	1RXS J130258.8+162423	0.067	0.7	-	-	-	15.50	-	1	1.0 <sup>#</sup>
65	NGC5033	1RXP J131327.7+363536	0.003	41.0	-	-	-	12.37	1	1	1.0
66	Mkn1347	1RXS J132254.2+081011	0.050	1.9	-	-	-	14.38	-	2	1.0
67	NGC5273	1RXP J134208.3+353919	0.003	10.0	3.6	15.5	0.0580±0.0124	13.44	1	2	1.0
68	Mkn279	1RXH J135303.5+691830	0.031	2.7	1.3	3.6	0.1409±0.0334	14.45	1	1	1.0
69	Mkn662	1RXS J135405.7+232549	0.055	1.0	-	-	-	15.24	-	2	1.5
70	NGC5548	1RXP J141759.3+250811	0.017	5.0	-	-	-	13.46	1	1	1.5
71	Mkn684	1RXS J143104.8+281716	0.046	4.0	2.0	9.0	0.0310±0.0067	14.68	1	1	2.0 <sup>#</sup>
72	Mkn471	1RXP J142255.5+325111	0.034	3.6	-	-	-	14.42	1	1	1.9

Table C.1. *continued*

Nr.	name	ROSAT name	$z$	$D_p$	$D_c$	$S$	$Q$	$V$	id		Sy type
				mm	mm	mm		mag	point.	sur.	
73	Mkn474	1RXP J143452.1+483933	0.041	1.2	-	-	-	15.18	1	1	1.0
74	Mkn817	1RXP J143622.9+584737	0.033	2.1	-	-	-	13.79	1	1	1.0
75	Mkn1494	1RXP J150139.6+102521	0.031	2.5	0.7	7.1	0.0065±0.0014	15.50	1	-	1.0
76	Mkn841	1RXP J150401.4+102617	0.036	1.2	-	-	-	14.92	1	1	1.0
77	Mkn1392	1RXS J150556.3+034212	0.036	3.1	-	-	-	14.14	-	1	1.5
78	Mkn845	1RXS J150744.6+512709	0.042	2.8	-	-	-	14.21	-	1	1.0
79	IR1509-2107	1RXP J151159.6-211903	0.044	0.7	-	-	-	14.04	1	1	1.0 <sup>#</sup>
80	NGC5940	1RXS J153118.2+072713	0.033	2.6	-	-	-	14.20	-	1	1.0
81	Mkn290	1RXP J153552.8+575411	0.029	1.5	-	-	-	14.62	1	1	1.0
82	Mkn486	1RXP J153638.0+543336	0.039	1.0	-	-	-	14.68	1	2	1.0
83	Mkn291	1RXP J155507.6+191139	0.035	1.4	-	-	-	15.50	2	1	1.0 <sup>#</sup>
84	Mkn493	1RXP J155909.7+350154	0.031	3.1	-	-	-	15.06	1	1	1.5 <sup>#</sup>
85	NGC6104	1RXS J161630.6+354204	0.028	6.0	2.0	16.7	0.0089±0.0019	14.00	-	2	1.0
86	Mkn699	1RXP J162347.0+410433	0.034	0.9	-	-	-	15.19	2	2	1.2
87	Mkn885	1RXS J162948.3+672247	0.026	2.6	-	-	-	14.17	-	1	1.0
88	Mkn883	1RXP J162953.3+242640	0.038	1.2	-	-	-	14.43	1	1	1.9
89	NGC6212	1RXP J164322.5+394823	0.030	1.9	-	-	-	15.00	1	-	1.0
90	NGC6240	1RXP J165259.0+022406	0.024	5.0	-	-	-	13.37	1	1	3.0
91	Mkn506	1RXP J172239.8+305245	0.043	2.3	1.7	3.7	0.1526±0.0360	14.55	1	1	1.5
92	NGC6814	1RXP J194240.7-101928	0.005	7.8	-	-	-	14.37	1	1	1.0
93	Mkn896	1RXP J204620.8-024848	0.027	2.3	0.7	6.0	0.0095±0.0021	14.28	1	1	1.0 <sup>#</sup>
94	Mkn516	1RXP J215622.2+072213	0.028	1.7	1.0	3.6	0.0475±0.0113	15.01	1	-	1.8
95	Mkn915	1RXS J223647.3-123228	0.025	3.4	2.1	9.8	0.0203±0.0044	14.03	-	2	1.5
96	IR2237+0747	1RXH J224017.3+080314	0.025	3.5	-	-	-	14.00	1	1	1.0
97	Mkn1126	1RXS J230048.1-125518	0.010	2.5	-	-	-	14.11	-	1	1.0 <sup>#</sup>
98	NGC7469	1RXP J230315.6+085233	0.017	3.0	2.7	6.3	0.0922±0.0203	13.72	1	1	1.0
99	Mkn315	1RXS J230402.8+223725	0.040	1.4	0.8	2.4	0.0857±0.0227	14.09	1	1	1.0
100	NGC7603	1RXP J231856.6+001448	0.029	4.2	0.8	4.8	0.0557±0.0126	14.21	1	1	1.0
101	Mkn541	1RXS J235602.1+073121	0.040	1.2	-	-	-	15.15	-	2	1.0
102	Mkn543	1RXS J000226.6+032105	0.026	2.0	-	-	-	14.09	-	1	1.0

Table C.2. **Seyfert2 galaxies:** A part of the Rafanelli sample of interacting or isolated Seyfert 2 galaxies detected by *ROSAT*. The table contains optical and general properties as well as some results from the investigations of Rafanelli et al. (1995). For the description of columns see table C.1.

Nr.	name	ROSAT name	$z$	$D_p$	$D_c$	$S$	$Q$	$V$	id		Sy type
				mm	mm	mm		mag	point.	sur.	
1	Mkn348	1RXP J004847.4+315716	0.014	2.0	0.5	5.0	0.0080±0.0018	14.59	1	-	2.0
2	IR0135-1307	1RXP J013805.4-125213	0.041	1.6	-	-	-	15.30	1	-	2.0
3	Mkn573	1RXP J014357.8+022050	0.017	2.3	-	-	-	14.07	1	1	2.0
4	IR0147-0740	1RXP J015002.7-072540	0.017	1.0	-	-	-	15.62	1	-	2.0
5	NGC1068	1RXP J024240.9-000042	0.003	28.0	-	-	-	10.83	1	1	2.0
6	NGC1144	1RXP J025511.9-001042	0.029	3.2	1.5	2.4	0.7607±0.2015	14.41	2	-	2.0
7	IR0253-1641	1RXS J025601.7-162919	0.033	1.7	-	-	-	15.50	-	1	2.0
8	Mkn1066	1RXS J025601.7-162919	0.012	4.2	-	-	-	13.96	1	-	2.0
9	Mkn607	1RXS J032446.8-030256	0.009	2.5	6.0	7.5	0.1377±0.0300	14.00	-	1	2.0
10	IR0450-0317	1WGA J0452.7-0312	0.016	2.0	-	-	-	15.00	2	-	2.0
11	NGC2110	1RXH J055211.4-072725	0.007	2.5	-	-	-	13.51	1	1	2.0
12	Mkn3	1RXP J061535.6+710209	0.014	3.5	-	-	-	13.34	1	2	2.0
13	Mkn620	1RXP J061535.6+710209	0.006	5.0	-	-	-	13.54	1	-	2.0
14	Mkn78	1RXP J074241.2+651031	0.038	1.6	-	-	-	14.58	1	-	2.0
15	Mkn1210	1RXS J080404.6+050641	0.013	2.2	-	-	-	15.00	-	2	2.0
16	NGC3081	1RXS J095930.3-224954	0.007	6.1	1.3	8.8	0.0328±0.0071	13.55	-	2	2.0
17	Mkn720	1RXS J101737.6+065820	0.045	1.6	-	-	-	15.27	-	1	2.0
18	Mkn34	1RXP J101737.6+065820	0.051	1.4	-	-	-	14.65	1	-	2.0
19	NGC3660	1RXS J112332.4-083932	0.011	6.5	-	-	-	14.45	-	1	2.0
20	NGC3982	1RXP J115628.0+550731	0.003	6.9	-	-	-	11.70	1	-	2.0
21	NGC4388	1RXP J122546.7+123946	0.008	16.0	2.3	39.0	0.0038±0.0008	13.90	1	-	2.0
22	NGC4922B	1RXP J122546.7+123946	0.024	4.3	-	-	-	15.00	1	-	2.0
23	NGC4941	1RXS J130413.2-053304	0.003	11.0	-	-	-	12.23	-	1	2.0
24	NGC5005	1RXP J131056.3+370323	0.003	23.0	-	-	-	13.67	1	1	2.0
25	IR1329+0216	1RXP J133152.2+020057	0.086	1.0	-	-	-	15.00	2	1	2.0
26	NGC5252	1RXP J133152.2+020057	0.022	4.2	0.7	8.9	0.0072±0.0015	14.21	1	-	2.0
27	Mkn266SW	1RXP J133818.7+481641	0.028	2.5	-	-	-	13.42	1	1	2.0
28	NGC5506	1RXP J141315.0-031218	0.007	8.9	3.5	12.5	0.0890±0.0191	14.38	1	1	2.0
29	Mkn670	1RXS J141417.5+264441	0.035	1.5	-	-	-	14.68	2	2	2.0
30	Mkn673	1RXP J141721.4+265141	0.036	4.5	-	-	-	15.00	1	-	2.0
31	NGC5929	1RXP J152607.0+414016	0.008	5.2	-	-	-	14.00	1	-	2.0
32	NGC5953	1RXH J153432.8+151137	0.007	4.7	5.5	3.5	3.0654±0.7308	13.10	1	1	2.0
33	NGC6211	1RXS J164118.4+574601	0.020	6.5	2.5	10.0	0.0655±0.0141	14.30	-	2	2.0
34	NGC7319	1RXH J223603.2+335833	0.022	3.5	4.8	6.2	0.2889±0.0638	13.53	1	2	2.0
35	NGC7674	1RXP J232757.0+084644	0.029	4.0	2.0	11.0	0.0170±0.0037	14.36	1	-	2.0
36	NGC7743	1RXP J232757.0+084644	0.007	8.0	-	-	-	13.28	2	-	2.0

**Table C.3. Seyfert1 galaxies:** The table contains soft X-ray properties of the interacting or isolated Seyfert 1 galaxies. Col(1) - object name, col(2&3) - ROSAT position (pointed observations are preferred), col(4&5) - pointing (p = PSPC, h = HRI detector), survey (RASS II catalogue) count rates, col(6&7) - exposure times, col(8&9) - logarithmic fluxes (f = from fit, c = from count rate), col(10&11) - logarithmic luminosities, col(12&13) - galactic and spectral hydrogen column densities ( $\equiv$  fixed value for  $N_{\text{H,fit}} < N_{\text{H,gal}}$  or no spectral  $\Gamma$ ), col(14) - monochromatic flux at 1keV and col(15) - photon index. In columns 2,3,13,14 and 15 we have preferred the data from the pointed spectral fit opposed to the survey spectral fit. Note that PSPC and HRI count rates are not comparable and see the discussion about column densities of Seyfert 2 in Sect. 3.2.2.

name	ROSAT position			count rate		$t_{\text{expo}}$		$\log f_X$		$\log L_X$		$N_{\text{H}}$		$f_{1\text{keV}}$	$\Gamma$
	$\alpha_{2000}$		$\delta_{2000}$	[counts s $^{-1}$ ]		[s]		[erg cm $^{-2}$ s $^{-1}$ ]		[erg s $^{-1}$ ]		[10 $^{21}$ cm $^{-2}$ ]		[10 $^{-5}$ phot s $^{-1}$ ]	
	[h]	[m]	[s]	[ $^{\circ}$ ]	[ $'$ ]	[ $''$ ]	point.	sur.	point.	sur.	point.	sur.	gal	fit	
Mkn334	00 03 08.6	21 57 28	-	-	0.096 $\pm$ 0.020	-	293	-	-11.59 $^c$	-	42.38	0.443	-	-	$\equiv$ -2.30
Mkn335	00 06 19.2	20 12 25	2.762 $\pm$ 0.011 $^P$	2.482 $\pm$ 0.097	24337	269	-9.95 $^f$	-9.81 $^f$	44.14	44.28	0.396	0.396 $\pm$ 0.016	682.74 $\pm$ 8.47	-3.04 $\pm$ 0.01	
Mkn1146	00 47 19.4	14 42 15	-	0.067 $\pm$ 0.015	-	370	-	-11.74 $^c$	-	42.73	0.460	-	-	$\equiv$ -2.30	
Mkn352	00 59 53.3	31 49 48	0.093 $\pm$ 0.005 $^P$	0.615 $\pm$ 0.037	4418	462	-11.63 $^f$	-10.73 $^f$	42.01	42.91	0.549	0.651 $\pm$ 0.136	47.65 $\pm$ 15.86	-1.94 $\pm$ 0.43	
Mkn1152	01 13 50.1	-14 50 34	1.923 $\pm$ 0.024 $^P$	0.946 $\pm$ 0.050	3219	412	-10.49 $^f$	-10.98 $^f$	44.24	43.74	0.163	0.209 $\pm$ 0.026	421.55 $\pm$ 16.33	-2.45 $\pm$ 0.10	
Mkn993	01 25 31.4	32 08 00	-	0.083 $\pm$ 0.017	-	328	-	-11.59 $^c$	-	42.15	0.571	-	-	$\equiv$ -2.30	
Mkn975	01 13 50.4	13 15 34	-	0.030 $\pm$ 0.012	-	462	-	-12.14 $^c$	-	42.56	0.390	-	-	$\equiv$ -2.30	
Mkn358	01 26 34.2	31 36 59	-	0.172 $\pm$ 0.026	-	303	-	-10.89 $^f$	-	43.66	0.602	$\equiv$ 0.602	69.30 $\pm$ 19.90	-3.12 $\pm$ 0.39	
Mkn359	01 27 32.8	19 10 51	0.822 $\pm$ 0.016 $^P$	0.608 $\pm$ 0.042	3187	388	-10.53 $^f$	-10.37 $^f$	43.22	43.38	0.483	0.543 $\pm$ 0.068	356.61 $\pm$ 16.21	-2.51 $\pm$ 0.13	
Mkn1018	02 06 16.0	-00 17 32	0.239 $\pm$ 0.006 $^P$	0.081 $\pm$ 0.017	6510	395	-11.26 $^f$	-11.83 $^c$	43.30	42.73	0.255	0.342 $\pm$ 0.073	81.50 $\pm$ 5.20	-2.33 $\pm$ 0.18	
Mkn590	02 14 33.7	-00 46 04	5.225 $\pm$ 0.039 $^P$	2.689 $\pm$ 0.167	3484	311	-9.89 $^f$	-10.30 $^f$	44.27	43.85	0.272	0.317 $\pm$ 0.020	1459.10 $\pm$ 29.21	-2.58 $\pm$ 0.05	
Mkn1040	02 28 14.6	31 18 38	-	0.342 $\pm$ 0.033	-	334	-	-11.20 $^f$	-	42.48	0.674	$\equiv$ 0.674	160.00 $\pm$ 30.80	-0.83 $\pm$ 0.64	
Mkn1044	02 30 05.8	-08 59 40	2.119 $\pm$ 0.027 $^P$	2.141 $\pm$ 0.128	2836	278	-10.02 $^f$	-10.12 $^f$	43.68	43.58	0.316	0.421 $\pm$ 0.040	549.43 $\pm$ 19.71	-3.08 $\pm$ 0.09	
NGC985	02 34 37.9	-08 47 09	1.331 $\pm$ 0.015 $^P$	1.281 $\pm$ 0.070	6191	267	-10.43 $^f$	-10.41 $^f$	44.14	44.16	0.283	0.342 $\pm$ 0.032	360.98 $\pm$ 10.91	-2.69 $\pm$ 0.08	
Mkn595	02 41 35.2	07 11 17	-	0.147 $\pm$ 0.029	-	198	-	-11.31 $^c$	-	42.88	0.676	-	-	$\equiv$ -2.30	
Mkn372	02 49 20.6	19 18 22	0.282 $\pm$ 0.005 $^P$	0.234 $\pm$ 0.026	12675	368	-10.91 $^f$	-10.76 $^f$	43.36	43.52	0.962	$\equiv$ 0.962	173.41 $\pm$ 4.63	-2.37 $\pm$ 0.07	
Mkn609	03 25 25.5	-06 08 27	0.181 $\pm$ 0.006 $^P$	0.413 $\pm$ 0.034	5801	400	-11.27 $^f$	-10.81 $^f$	43.03	43.50	0.456	0.585 $\pm$ 0.116	93.81 $\pm$ 7.12	-2.14 $\pm$ 0.26	
Mkn618	04 36 22.1	-10 22 31	0.316 $\pm$ 0.010 $^h$	0.579 $\pm$ 0.042	3001	370	-10.41 $^c$	-10.69 $^f$	43.97	43.69	0.583	$\equiv$ 0.583	210.00 $\pm$ 30.70	-2.64 $\pm$ 0.27	
Mkn6	06 52 09.8	74 25 37	-	0.062 $\pm$ 0.012	-	451	-	-11.69 $^c$	-	42.15	0.646	-	-	$\equiv$ -2.30	
Mkn374	06 59 38.5	54 11 36	-	0.775 $\pm$ 0.050	-	333	-	-10.28 $^f$	-	44.31	0.618	$\equiv$ 0.618	249.00 $\pm$ 37.60	-3.20 $\pm$ 0.19	
Mkn9	07 36 57.0	58 46 10	-	0.130 $\pm$ 0.022	-	308	-	-11.45 $^c$	-	43.03	0.469	-	-	$\equiv$ -2.30	
Mkn79	07 42 33.5	49 48 38	1.752 $\pm$ 0.026 $^P$	2.196 $\pm$ 0.076	2690	383	-9.99 $^f$	-9.94 $^f$	43.99	44.03	0.566	0.790 $\pm$ 0.060	1039.90 $\pm$ 33.85	-2.66 $\pm$ 0.10	
Mkn10	07 47 28.6	60 55 53	0.981 $\pm$ 0.015 $^P$	0.586 $\pm$ 0.040	4246	409	-10.49 $^f$	-10.69 $^f$	43.75	43.56	0.482	$\equiv$ 0.482	390.60 $\pm$ 11.51	-2.51 $\pm$ 0.04	
Mkn382	07 55 25.1	39 11 13	0.122 $\pm$ 0.006 $^h$	0.449 $\pm$ 0.034	3535	425	-10.65 $^c$	-10.58 $^f$	43.71	43.78	0.532	$\equiv$ 0.532	146.00 $\pm$ 26.90	-3.09 $\pm$ 0.23	
Mkn1218	08 38 10.8	24 53 37	0.473 $\pm$ 0.013 $^P$	0.213 $\pm$ 0.028	2879	310	-11.02 $^f$	-11.31 $^c$	43.15	42.87	0.354	0.449 $\pm$ 0.045	235.21 $\pm$ 49.80	-1.50 $\pm$ 0.22	
NGC2639	08 43 38.0	50 12 08	0.023 $\pm$ 0.002 $^P$	-	8749	-	-12.41 $^f$	-	40.95	-	0.316	$\equiv$ 0.316	6.62 $\pm$ 1.09	-2.16 $\pm$ 0.24	
NGC2782	09 14 05.0	40 06 48	0.011 $\pm$ 0.001 $^h$	-	21715	-	-12.19 $^c$	-	40.90	-	0.180	-	-	$\equiv$ -2.30	
Mkn704	09 18 26.2	16 18 25	-	0.756 $\pm$ 0.051	-	321	-	-10.61 $^f$	-	43.61	0.347	0.407 $\pm$ 0.237	219.00 $\pm$ 40.40	-2.76 $\pm$ 0.52	
Mkn110	09 25 12.8	52 17 13	6.496 $\pm$ 0.033 $^P$	1.691 $\pm$ 0.063	6013	441	-9.97 $^f$	-10.63 $^f$	44.44	43.78	0.156	0.193 $\pm$ 0.010	1181.2 $\pm$ 20.23	-2.59 $\pm$ 0.04	
Mkn705	09 26 03.0	12 44 00	1.001 $\pm$ 0.014 $^P$	1.246 $\pm$ 0.088	5244	347	-10.54 $^f$	-10.44 $^f$	43.65	43.75	0.351	0.398 $\pm$ 0.042	342.95 $\pm$ 11.86	-2.53 $\pm$ 0.09	
NGC2992	09 45 41.6	-14 19 39	0.121 $\pm$ 0.003 $^P$	0.284 $\pm$ 0.029	18586	394	-11.41 $^f$	-11.08 $^c$	41.56	41.89	0.517	2.101 $\pm$ 1.471	72.41 $\pm$ 54.60	-0.87 $\pm$ 0.36	
Mkn124	09 48 41.6	50 29 26	-	0.028 $\pm$ 0.010	-	522	-	-12.57 $^c$	-	42.22	0.090	-	-	$\equiv$ -2.30	
Mkn1239	09 52 19.0	-01 36 32	0.069 $\pm$ 0.003 $^P$	0.054 $\pm$ 0.014	9043	418	-10.69 $^f$	-11.89 $^c$	43.17	41.96	0.384	0.859 $\pm$ 0.170	22.42 $\pm$ 2.34	-4.06 $\pm$ 0.30	
NGC3031	09 55 32.8	69 03 54	0.733 $\pm$ 0.005 $^P$	0.998 $\pm$ 0.088	28086	140	-10.59 $^f$	-10.45 $^f$	40.60	40.74	0.427	0.712 $\pm$ 0.032	396.29 $\pm$ 6.19	-2.28 $\pm$ 0.07	
NGC3080	09 59 56.2	13 02 43	0.300 $\pm$ 0.017 $^P$	0.219 $\pm$ 0.031	1080	255	-11.10 $^f$	-11.32 $^c$	43.28	43.06	0.329	0.367 $\pm$ 0.163	92.95 $\pm$ 13.66	-2.54 $\pm$ 0.39	
NGC3185	10 17 37.8	21 41 24	0.005 $\pm$ 0.001 $^P$	-	4617	-	-12.95 $^f$	-	39.53	-	0.216	0.279 $\pm$ 0.894	1.42 $\pm$ 1.14	-2.47 $\pm$ 2.64	
Mkn141	10 19 12.1	63 58 02	0.032 $\pm$ 0.003 $^h$	0.506 $\pm$ 0.036	3589	498	-11.73 $^c$	-11.15 $^f$	42.75	43.33	0.107	0.146 $\pm$ 0.123	82.00 $\pm$ 22.60	-2.56 $\pm$ 0.62	
NGC3227	10 23 30.2	19 51 50	0.560 $\pm$ 0.005 $^P$	0.099 $\pm$ 0.020	19547	279	-11.00 $^f$	-11.78 $^c$	41.24	40.45	0.222	0.396 $\pm$ 0.013	259.21 $\pm$ 25.76	-1.25 $\pm$ 0.08	
Mkn142	10 25 32.5	51 40 46	1.373 $\pm$ 0.013 $^P$	1.747 $\pm$ 0.059	8427	549	-10.41 $^f$	-10.69 $^f$	44.21	43.93	0.118	0.252 $\pm$ 0.026	163.55 $\pm$ 8.19	-3.28 $\pm$ 0.09	
Mkn634	10 58 01.2	20 29 37	-	0.164 $\pm$ 0.029	-	236	-	-11.62 $^c$	-	43.32	0.186	-	-	$\equiv$ -2.30	
NGC3516	11 06 49.0	72 34 07	4.711 $\pm$ 0.019 $^P$	0.140 $\pm$ 0.020	13079	431	-9.93 $^f$	-11.38 $^f$	43.26	41.81	0.355	$\equiv$ 0.355	1595.40 $\pm$ 13.08	-2.40 $\pm$ 0.01	
Mkn732	11 13 49.5	09 35 18	-	0.268 $\pm$ 0.026	-	425	-	-11.03 $^f$	-	43.22	0.235	0.438 $\pm$ 0.407	98.30 $\pm$ 28.30	-2.64 $\pm$ 0.96	
Mkn734	11 21 46.9	11 44 18	0.450 $\pm$ 0.011 $^P$	0.418 $\pm$ 0.032	4011	439	-10.48 $^f$	-11.02 $^f$	44.22	43.67	0.264	0.450 $\pm$ 0.083	77.07 $\pm$ 6.35	-3.63 $\pm$ 0.19	
Mkn40	11 25 36.6	54 23 03	0.459 $\pm$ 0.007 $^P$	0.101 $\pm$ 0.020	8707	383	-11.21 $^f$	-11.98 $^c$	42.67	41.91	0.106	0.155 $\pm$ 0.031	134.72 $\pm$ 5.77	-1.80 $\pm$ 0.12	
Mkn739A	11 36 29.2	21 35 43	0.703 $\pm$ 0.010 $^P$	0.487 $\pm$ 0.034	7553	435	-10.50 $^f$	-11.02 $^f$	43.74	43.21	0.186	0.932 $\pm$ 0.077	420.77 $\pm$ 12.46	-2.43 $\pm$ 0.14	
Mkn744	11 39 42.8	31 54 39	0.391 $\pm$ 0.012 $^P$	0.034 $\pm$ 0.014	2866	286	-11.10 $^f$	-12.29 $^c$	42.18	40.99	0.192	0.652 $\pm$ 0.283	206.54 $\pm$ 61.30	-1.00 $\pm$ 0.18	
NGC3884	11 46 11.5	20 23 55	-	0.048 $\pm$ 0.013	-	453	-	-12.11 $^c$	-	41.90	0.214	-	-	$\equiv$ -2.30	
Mkn42	11 53 41.7	46 12 55	0.240 $\pm$ 0.007 $^P$	0.192 $\pm$ 0.027	4429	308	-11.24 $^f$	-11.36 $^f$	42.81	42.69	0.199	0.283 $\pm$ 0.080	51.68 $\pm$ 4.98	-2.76 $\pm$ 0.23	
Mkn1310	12 01 14.9	-03 40 31	0.188 $\pm$ 0.004 $^P$	0.831 $\pm$ 0.073	13559	339	-11.43 $^f$	-10.82 $^f$	42.41	43.02	0.243	0.303 $\pm$ 0.056	64.60 $\pm$ 3.38	-2.13 $\pm$ 0.16	

Table C.3. *continued*

name	ROSAT position		count rate		$t_{\text{expo}}$		$\log f_X$		$\log L_X$		$N_{\text{H}}$		$f_{1\text{keV}}$	$\Gamma$
	$\alpha_{2000}$ [h] [m] [s]	$\delta_{2000}$ [ $^{\circ}$ ] [ $'$ ] [ $''$ ]	[counts s $^{-1}$ ]		point.	sur.	point.	sur.	point.	sur.	gal	fit	[10 $^{-5}$ phot s $^{-1}$ ] cm $^{-2}$ keV $^{-1}$ ]	
NGC4051	12 03 10.2	44 31 56	1.903 $\pm$ 0.008 <sup>P</sup>	3.918 $\pm$ 0.108	28459	342	-10.42 <sup>f</sup>	-10.16 <sup>f</sup>	41.46	41.72	0.137	0.235 $\pm$ 0.011	229.49 $\pm$ 4.21	-3.04 $\pm$ 0.04
NGC4151	12 10 32.4	39 24 19	0.600 $\pm$ 0.004 <sup>P</sup>	0.224 $\pm$ 0.025	36337	449	-10.89 <sup>f</sup>	-10.87 <sup>f</sup>	41.34	41.37	0.208	0.282 $\pm$ 0.019	162.90 $\pm$ 3.14	-2.46 $\pm$ 0.06
Mkn1469	12 16 07.4	50 49 26	-	0.079 $\pm$ 0.017	-	317	-	-11.93 <sup>c</sup>	-	42.34	0.187	-	-	$\equiv$ -2.30
NGC4235	12 17 10.1	07 11 35	0.184 $\pm$ 0.004 <sup>P</sup>	0.104 $\pm$ 0.017	10293	425	-11.11 <sup>f</sup>	-11.87 <sup>c</sup>	41.86	41.10	0.152	2.091 $\pm$ 0.263	154.50 $\pm$ 96.08	-1.96 $\pm$ 0.60
Mkn766	12 18 26.4	29 48 48	3.851 $\pm$ 0.014 <sup>P</sup>	4.710 $\pm$ 0.113	19856	377	-10.05 <sup>f</sup>	-9.80 <sup>f</sup>	43.39	43.64	0.169	0.286 $\pm$ 0.010	930.08 $\pm$ 10.23	-2.63 $\pm$ 0.03
NGC4258	12 18 56.4	47 17 56	0.357 $\pm$ 0.004 <sup>P</sup>	0.195 $\pm$ 0.021	25736	431	-10.42 <sup>f</sup>	-10.67 <sup>f</sup>	41.47	41.21	0.120	0.713 $\pm$ 0.053	121.04 $\pm$ 3.96	-3.46 $\pm$ 0.10
NGC4278	12 20 07.2	29 16 46	0.055 $\pm$ 0.004 <sup>P</sup>	0.037 $\pm$ 0.012	3411	381	-11.41 <sup>f</sup>	-12.28 <sup>c</sup>	40.47	39.60	0.172	0.682 $\pm$ 0.313	20.08 $\pm$ 3.87	-3.14 $\pm$ 0.54
Mkn205	12 21 44.5	75 18 40	0.780 $\pm$ 0.010 <sup>P</sup>	0.864 $\pm$ 0.045	7435	455	-10.73 <sup>f</sup>	-10.89 <sup>f</sup>	44.27	44.09	0.280	0.350 $\pm$ 0.038	265.16 $\pm$ 8.84	-2.37 $\pm$ 0.09
Mkn50	12 23 24.4	02 40 40	-	0.070 $\pm$ 0.017	-	326	-	-11.12 <sup>f</sup>	-	42.88	0.176	$\equiv$ 0.176	142.00 $\pm$ 27.00	-2.04 $\pm$ 0.20
NGC4593	12 39 39.2	-05 20 46	1.472 $\pm$ 0.034 <sup>P</sup>	3.432 $\pm$ 0.170	1261	126	-10.58 <sup>f</sup>	-10.25 <sup>f</sup>	42.61	42.94	0.228	0.248 $\pm$ 0.055	424.54 $\pm$ 26.58	-2.23 $\pm$ 0.17
NGC4594	12 39 59.2	-11 37 31	0.134 $\pm$ 0.004 <sup>P</sup>	0.108 $\pm$ 0.022	10567	282	-11.44 <sup>f</sup>	-11.58 <sup>c</sup>	40.44	40.30	0.385	0.637 $\pm$ 0.065	68.89 $\pm$ 19.86	-2.02 $\pm$ 0.27
NGC4639	12 42 52.2	13 15 28	0.035 $\pm$ 0.002 <sup>P</sup>	0.161 $\pm$ 0.022	6604	389	-12.20 <sup>f</sup>	-11.55 <sup>c</sup>	39.08	39.73	0.236	0.312 $\pm$ 0.207	10.25 $\pm$ 1.91	-2.22 $\pm$ 0.68
IR1249-1308	12 52 12.5	-13 24 50	-	0.969 $\pm$ 0.060	-	294	-	-10.67 <sup>f</sup>	-	42.91	0.358	$\equiv$ 0.358	265.00 $\pm$ 39.40	-2.50 $\pm$ 0.17
Mkn236	13 00 21.2	61 39 19	-	0.202 $\pm$ 0.022	-	524	-	-11.52 <sup>f</sup>	-	43.20	0.183	$\equiv$ 0.183	51.50 $\pm$ 13.70	-2.16 $\pm$ 0.27
Mkn783	13 02 58.8	16 24 23	-	0.288 $\pm$ 0.034	-	580	-	-11.22 <sup>f</sup>	-	43.70	0.197	0.455 $\pm$ 0.143	154.0 $\pm$ 147.00	-1.30 $\pm$ 0.72
NGC5033	13 13 27.7	36 35 37	0.277 $\pm$ 0.007 <sup>P</sup>	0.338 $\pm$ 0.027	5076	542	-11.30 <sup>f</sup>	-11.29 <sup>f</sup>	40.94	40.95	0.094	0.250 $\pm$ 0.067	90.43 $\pm$ 6.21	-2.10 $\pm$ 0.24
Mkn1347	13 22 54.2	08 10 11	-	0.083 $\pm$ 0.022	-	270	-	-11.89 <sup>c</sup>	-	42.80	0.199	-	-	$\equiv$ -2.30
NGC5273	13 42 08.3	35 39 20	0.027 $\pm$ 0.002 <sup>P</sup>	0.021 $\pm$ 0.008	5386	668	-12.52 <sup>f</sup>	-12.69 <sup>c</sup>	39.72	39.55	0.093	0.141 $\pm$ 0.180	4.94 $\pm$ 1.52	-2.23 $\pm$ 0.81
Mkn279	13 53 03.5	69 18 30	1.177 $\pm$ 0.017 <sup>h</sup>	2.809 $\pm$ 0.070	4298	612	-10.20 <sup>c</sup>	-10.41 <sup>f</sup>	44.07	43.86	0.177	0.177 $\pm$ 0.050	674.00 $\pm$ 53.30	-2.13 $\pm$ 0.21
Mkn662	13 54 05.7	23 25 49	-	0.117 $\pm$ 0.022	-	326	-	-11.78 <sup>c</sup>	-	43.00	0.177	-	-	$\equiv$ -2.30
NGC5548	14 17 59.3	25 08 11	5.889 $\pm$ 0.023 <sup>P</sup>	4.954 $\pm$ 0.105	10946	458	-10.02 <sup>f</sup>	-10.21 <sup>f</sup>	43.72	43.54	0.193	0.193 $\pm$ 0.008	1278.60 $\pm$ 15.38	-2.41 $\pm$ 0.03
Mkn684	14 31 04.6	28 17 17	0.245 $\pm$ 0.009 <sup>h</sup>	0.577 $\pm$ 0.041	2835	388	-10.63 <sup>c</sup>	-10.87 <sup>f</sup>	43.99	43.76	0.150	0.267 $\pm$ 0.170	105.00 $\pm$ 25.40	-2.86 $\pm$ 0.53
Mkn471	14 22 55.5	32 51 11	0.028 $\pm$ 0.002 <sup>P</sup>	0.028 $\pm$ 0.009	8971	562	-12.42 <sup>f</sup>	-12.52 <sup>c</sup>	41.92	41.83	0.113	0.117 $\pm$ 0.151	9.02 $\pm$ 1.71	-1.60 $\pm$ 0.60
Mkn474	14 34 52.1	48 39 34	0.874 $\pm$ 0.008 <sup>P</sup>	0.248 $\pm$ 0.020	12808	774	-10.73 <sup>f</sup>	-10.76 <sup>f</sup>	43.79	43.78	0.201	0.311 $\pm$ 0.025	307.97 $\pm$ 7.32	-2.20 $\pm$ 0.07
Mkn817	14 36 22.9	58 47 38	0.470 $\pm$ 0.010 <sup>P</sup>	0.102 $\pm$ 0.017	4679	542	-11.22 <sup>f</sup>	-11.46 <sup>f</sup>	43.11	42.87	0.154	$\equiv$ 0.154	91.61 $\pm$ 5.26	-2.30 $\pm$ 0.05
Mkn1494	15 01 39.6	10 25 22	0.006 $\pm$ 0.001 <sup>P</sup>	-	3638	-	-12.84 <sup>c</sup>	-	41.43	-	0.224	-	-	$\equiv$ -2.30
Mkn841	15 04 01.4	10 26 17	2.238 $\pm$ 0.012 <sup>P</sup>	0.810 $\pm$ 0.054	16842	311	-10.35 <sup>f</sup>	-10.90 <sup>f</sup>	44.06	43.50	0.224	0.255 $\pm$ 0.012	544.91 $\pm$ 8.19	-2.51 $\pm$ 0.04
Mkn1392	15 05 56.3	03 42 12	-	0.027 $\pm$ 0.011	-	390	-	-12.19 <sup>c</sup>	-	42.21	0.374	-	-	$\equiv$ -2.30
Mkn845	15 07 44.6	51 27 09	-	0.242 $\pm$ 0.018	-	887	-	-11.55 <sup>f</sup>	-	42.99	0.183	$\equiv$ 0.183	52.30 $\pm$ 8.37	-2.06 $\pm$ 0.17
IR1509-2107	15 11 59.7	-21 19 00	0.286 $\pm$ 0.010 <sup>P</sup>	0.067 $\pm$ 0.015	2736	360	-10.50 <sup>f</sup>	-10.86 <sup>f</sup>	44.08	43.70	0.792	3.490 $\pm$ 0.474	339.41 $\pm$ 275.20	-2.61 $\pm$ 1.04
NGC5940	15 31 18.2	07 27 13	-	0.254 $\pm$ 0.036	-	253	-	-11.09 <sup>f</sup>	-	43.23	0.381	$\equiv$ 0.381	128.00 $\pm$ 34.10	-2.25 $\pm$ 0.41
Mkn290	15 35 52.8	57 54 12	0.592 $\pm$ 0.010 <sup>P</sup>	0.885 $\pm$ 0.031	5999	1061	-10.97 <sup>f</sup>	-10.82 <sup>f</sup>	43.25	43.39	0.178	0.251 $\pm$ 0.041	159.87 $\pm$ 7.46	-2.32 $\pm$ 0.13
Mkn486	15 36 38.0	54 33 37	0.011 $\pm$ 0.002 <sup>P</sup>	0.003 $\pm$ 0.002	2792	1179	-12.98 <sup>f</sup>	-13.46 <sup>c</sup>	41.50	41.02	0.128	$\equiv$ 0.128	0.89 $\pm$ 0.87	-2.80 $\pm$ 0.76
Mkn291	15 55 07.6	19 11 40	0.065 $\pm$ 0.004 <sup>P</sup>	0.042 $\pm$ 0.011	3776	598	-11.30 <sup>f</sup>	-12.02 <sup>c</sup>	43.09	42.35	0.346	0.543 $\pm$ 0.425	17.01 $\pm$ 4.89	-3.41 $\pm$ 0.79
Mkn493	15 59 09.7	35 01 54	0.379 $\pm$ 0.007 <sup>P</sup>	0.516 $\pm$ 0.038	8038	399	-11.02 <sup>f</sup>	-10.98 <sup>f</sup>	43.26	43.29	0.222	0.295 $\pm$ 0.050	77.32 $\pm$ 4.57	-2.84 $\pm$ 0.14
NGC6104	16 16 30.6	35 42 04	-	0.011 $\pm$ 0.005	-	807	-	-12.88 <sup>c</sup>	-	41.30	0.133	-	-	$\equiv$ -2.30
Mkn699	16 23 47.0	41 04 34	0.033 $\pm$ 0.002 <sup>P</sup>	0.027 $\pm$ 0.008	10115	873	-12.46 <sup>f</sup>	-12.57 <sup>c</sup>	41.90	41.78	0.096	0.106 $\pm$ 0.149	2.29 $\pm$ 1.59	-2.98 $\pm$ 1.02
Mkn885	16 29 48.3	67 22 47	-	0.194 $\pm$ 0.011	-	1999	-	-11.30 <sup>f</sup>	-	42.82	0.378	$\equiv$ 0.378	92.20 $\pm$ 9.05	-2.08 $\pm$ 0.17
Mkn883	16 29 53.3	24 26 40	0.057 $\pm$ 0.004 <sup>P</sup>	0.041 $\pm$ 0.011	3229	502	-11.73 <sup>f</sup>	-11.99 <sup>c</sup>	42.71	42.46	0.403	1.418 $\pm$ 0.361	33.65 $\pm$ 66.16	-2.08 $\pm$ 1.62
NGC6212	16 43 22.5	39 48 23	0.009 $\pm$ 0.001 <sup>P</sup>	-	5982	-	-13.04 <sup>f</sup>	-	41.20	-	0.101	$\equiv$ 0.101	1.91 $\pm$ 0.71	-1.88 $\pm$ 0.40
NGC6240	16 52 59.0	02 24 07	0.055 $\pm$ 0.003 <sup>P</sup>	0.086 $\pm$ 0.016	5232	507	-10.71 <sup>f</sup>	-11.59 <sup>c</sup>	43.35	42.46	0.549	2.805 $\pm$ 1.412	50.48 $\pm$ 77.54	-3.58 $\pm$ 2.17
Mkn506	17 22 39.8	30 52 46	0.422 $\pm$ 0.015 <sup>P</sup>	1.526 $\pm$ 0.047	1922	747	-11.05 <sup>f</sup>	-10.47 <sup>f</sup>	43.51	44.09	0.328	$\equiv$ 0.328	145.87 $\pm$ 10.30	-2.20 $\pm$ 0.09
NGC6814	19 42 40.7	-10 19 29	0.061 $\pm$ 0.001 <sup>P</sup>	0.363 $\pm$ 0.035	38209	339	-11.68 <sup>f</sup>	-10.84 <sup>f</sup>	41.00	41.84	1.296	1.329 $\pm$ 0.110	42.37 $\pm$ 19.16	-1.93 $\pm$ 0.35
Mkn896	20 46 20.8	-02 48 48	0.475 $\pm$ 0.008 <sup>P</sup>	0.438 $\pm$ 0.040	6903	290	-10.38 <sup>f</sup>	-10.32 <sup>f</sup>	43.78	43.85	0.586	$\equiv$ 0.586	147.68 $\pm$ 6.04	-3.38 $\pm$ 0.05
Mkn516	21 56 22.2	07 22 13	0.013 $\pm$ 0.001 <sup>P</sup>	-	7109	-	-11.37 <sup>f</sup>	-	42.82	-	0.483	3.851 $\pm$ 0.847	16.91 $\pm$ 40.49	-3.32 $\pm$ 3.35
Mkn915	22 36 47.3	-12 32 28	-	0.123 $\pm$ 0.026	-	208	-	-11.46 <sup>c</sup>	-	42.62	0.491	-	-	$\equiv$ -2.30
IR2237+0747	22 40 17.2	08 03 17	0.088 $\pm$ 0.006 <sup>h</sup>	0.484 $\pm$ 0.051	2374	213	-11.09 <sup>c</sup>	-10.83 <sup>f</sup>	42.99	43.25	0.659	$\equiv$ 0.659	232.00 $\pm$ 44.50	-2.26 $\pm$ 0.49
Mkn1126	23 00 48.1	-12 55 18	-	0.350 $\pm$ 0.069	-	80	-	-11.10 <sup>c</sup>	-	42.18	0.352	-	-	$\equiv$ -2.30
NGC7469	23 03 15.6	08 52 33	1.772 $\pm$ 0.010 <sup>P</sup>	1.882 $\pm$ 0.144	18562	384	-10.21 <sup>f</sup>	-10.26 <sup>f</sup>	43.53	43.49	0.529	0.606 $\pm$ 0.021	871.34 $\pm$ 11.27	-2.37 $\pm$ 0.04
Mkn315	23 04 02.8	22 37 25	0.022 $\pm$ 0.002 <sup>h</sup>	0.132 $\pm$ 0.018	8298	465	-11.70 <sup>c</sup>	-11.25 <sup>f</sup>	42.80	43.25	0.574	0.578 $\pm$ 0.676	75.40 $\pm$ 28.10	-2.42 $\pm$ 1.68
NGC7603	23 18 56.6	00 14 48	0.532 $\pm$ 0.010 <sup>P</sup>	0.408 $\pm$ 0.049	5425	189	-10.88 <sup>f</sup>	-11.08 <sup>f</sup>	43.33	43.13	0.411	0.447 $\pm$ 0.060	236.65 $\pm$ 10.65	-2.09 $\pm$ 0.14
Mkn541	23 56 02.1	07 31 21	-	0.049 $\pm$ 0.013	-	417	-	-11.81 <sup>c</sup>	-	42.68	0.593	-	-	$\equiv$ -2.30
Mkn543	00 02 26.6	03 21 05	-	0.226 $\pm$ 0.027	-	402	-	-11.02 <sup>f</sup>	-	43.10	0.407	$\equiv$ 0.407	88.60 $\pm$ 21.60	-2.73 $\pm$ 0.29

**Table C.4. Seyfert2 galaxies:** The table contains soft X-ray properties of the interacting or isolated Seyfert 2 galaxies. For the description of columns see table C.3.

name	ROSAT position		count rate		$t_{\text{expo}}$		$\log f_X$		$\log L_X$		$N_{\text{H}}$		$f_{\text{1keV}}$	$\Gamma$
	$\alpha_{2000}$		[counts s $^{-1}$ ]		[s]		[erg cm $^{-2}$ s $^{-1}$ ]		[erg s $^{-1}$ ]		[10 $^{21}$ cm $^{-2}$ ]		[10 $^{-5}$ phot s $^{-1}$ ]	
	[h] [m] [s]	[ $^{\circ}$ ] [ $'$ ] [ $''$ ]	pointing	survey	point.	sur.	point.	sur.	point.	sur.	gal	fit	[cm $^{-2}$ keV $^{-1}$ ]	
Mkn348	00 48 47.4	31 57 16	0.010 $\pm$ 0.001 $^P$	-	23437	-	-12.52 $^f$	-	41.06	-	0.591	0.644 $\pm$ 0.334	3.98 $\pm$ 2.40	-2.43 $\pm$ 0.88
IR0135-1307	01 38 05.4	-12 52 14	0.010 $\pm$ 0.001 $^P$	-	6780	-	-11.41 $^f$	-	43.14	-	0.245	0.950 $\pm$ 0.674	2.41 $\pm$ 0.99	-4.36 $\pm$ 1.23
Mkn573	01 43 57.8	02 20 51	0.076 $\pm$ 0.002 $^P$	0.066 $\pm$ 0.016	13683	386	-11.40 $^f$	-11.88 $^c$	42.35	41.87	0.291	0.430 $\pm$ 0.107	15.85 $\pm$ 1.62	-3.32 $\pm$ 0.24
IR0147-0740	01 50 02.7	-07 25 40	0.040 $\pm$ 0.002 $^P$	-	6896	-	-11.71 $^f$	-	42.03	-	0.219	3.275 $\pm$ 3.520	43.43 $\pm$ 42.20	-1.77 $\pm$ 1.69
NGC1068	02 42 40.9	-00 00 43	1.957 $\pm$ 0.040 $^P$	1.785 $\pm$ 0.094	1211	206	-9.83 $^f$	-10.26 $^f$	42.41	41.97	0.355	0.524 $\pm$ 0.069	478.49 $\pm$ 28.30	-3.44 $\pm$ 0.14
NGC1144	02 55 11.9	-00 10 43	0.007 $\pm$ 0.001 $^P$	-	11855	-	-12.07 $^f$	-	42.16	-	0.619	0.879 $\pm$ 0.689	2.69 $\pm$ 0.97	-3.46 $\pm$ 1.14
IR0253-1641	02 56 01.7	-16 29 19	-	0.093 $\pm$ 0.021	-	277	-	-11.70 $^c$	-	42.63	0.322	-	-	$\equiv$ -2.30
Mkn1066	02 59 58.7	36 49 17	0.005 $\pm$ 0.001 $^h$	-	15605	-	-12.21 $^c$	-	41.23	-	1.185	-	-	$\equiv$ -2.30
Mkn607	03 24 49.0	-03 02 37	-	0.030 $\pm$ 0.013	-	341	-	-12.14 $^c$	-	41.05	0.397	-	-	$\equiv$ -2.30
IR0450-0317	04 52 44.0	-03 12 56	0.007 $\pm$ 0.001 $^P$	-	16025	-	-12.23 $^f$	-	41.47	-	0.437	0.794 $\pm$ 0.729	2.52 $\pm$ 0.89	-3.28 $\pm$ 1.63
NGC2110	05 52 11.6	-07 27 25	0.018 $\pm$ 0.001 $^h$	0.037 $\pm$ 0.010	31439	510	-11.59 $^c$	-11.72 $^c$	41.39	41.25	1.731	-	-	$\equiv$ -2.30
Mkn3	06 15 35.6	71 02 10	0.062 $\pm$ 0.002 $^P$	0.056 $\pm$ 0.014	21098	393	-10.63 $^f$	-11.68 $^c$	42.95	41.89	0.846	2.350 $\pm$ 1.190	56.82 $\pm$ 4.47	-3.61 $\pm$ 1.46
Mkn620	06 50 09.1	60 50 48	0.001 $\pm$ 0.000 $^h$	-	34465	-	-12.94 $^c$	-	39.90	-	0.731	-	-	$\equiv$ -2.30
Mkn78	07 42 41.2	65 10 32	0.009 $\pm$ 0.001 $^P$	-	14697	-	-11.22 $^f$	-	43.27	-	0.405	1.360 $\pm$ 0.709	4.08 $\pm$ 1.11	-4.32 $\pm$ 1.32
Mkn1210	08 04 06.1	05 07 04	-	0.030 $\pm$ 0.013	-	272	-	-12.21 $^c$	-	41.30	0.302	-	-	$\equiv$ -2.30
NGC3081	09 59 30.3	-22 49 54	-	0.022 $\pm$ 0.008	-	511	-	-12.22 $^c$	-	40.75	0.454	-	-	$\equiv$ -2.30
Mkn720	10 17 37.6	06 58 20	-	0.086 $\pm$ 0.016	-	434	-	-11.80 $^c$	-	42.80	0.256	-	-	$\equiv$ -2.30
Mkn34	10 34 08.3	60 01 55	0.006 $\pm$ 0.002 $^h$	-	1427	-	-12.57 $^c$	-	42.15	-	0.070	-	-	$\equiv$ -2.30
NGC3660	11 23 32.4	-08 39 32	-	0.061 $\pm$ 0.016	-	355	-	-11.84 $^c$	-	41.53	0.383	-	-	$\equiv$ -2.30
NGC3982	11 56 28.0	55 07 32	0.015 $\pm$ 0.002 $^P$	-	3851	-	-12.29 $^f$	-	39.94	-	0.122	0.374 $\pm$ 0.575	2.24 $\pm$ 1.30	-3.26 $\pm$ 1.38
NGC4388	12 25 46.7	12 39 46	0.049 $\pm$ 0.002 $^P$	-	11639	-	-11.07 $^f$	-	42.02	-	0.263	1.018 $\pm$ 0.376	19.68 $\pm$ 3.61	-3.64 $\pm$ 0.62
NGC4922B	13 01 25.3	29 18 43	0.003 $\pm$ 0.001 $^h$	-	17170	-	-12.88 $^c$	-	41.17	-	0.098	-	-	$\equiv$ -2.30
NGC4941	13 04 13.2	-05 33 04	-	0.035 $\pm$ 0.015	-	268	-	-12.20 $^c$	-	40.04	0.248	-	-	$\equiv$ -2.30
NGC5005	13 10 56.3	37 03 23	0.089 $\pm$ 0.003 $^P$	0.062 $\pm$ 0.013	9004	540	-11.30 $^f$	-12.17 $^c$	40.94	40.06	0.111	0.558 $\pm$ 0.155	27.44 $\pm$ 2.97	-3.12 $\pm$ 0.31
IR1329+0216	13 31 52.2	02 00 57	0.011 $\pm$ 0.001 $^P$	-	9791	-	-12.09 $^f$	-	43.14	-	0.185	0.373 $\pm$ 0.510	1.12 $\pm$ 0.90	-3.93 $\pm$ 1.44
NGC5252	13 38 16.0	04 32 31	0.003 $\pm$ 0.001 $^h$	-	3745	-	-12.69 $^c$	-	41.28	-	0.197	-	-	$\equiv$ -2.30
Mkn266SW	13 38 18.7	48 16 42	0.039 $\pm$ 0.002 $^P$	0.043 $\pm$ 0.011	9807	562	-11.81 $^f$	-12.22 $^c$	42.38	41.96	0.174	0.410 $\pm$ 0.177	9.52 $\pm$ 1.56	-3.04 $\pm$ 0.40
NGC5506	14 13 15.0	-03 12 18	0.292 $\pm$ 0.008 $^P$	0.106 $\pm$ 0.019	4380	366	-10.92 $^c$	-11.58 $^c$	42.05	41.40	0.405	>1.000	4070 $\pm$ 634	$\equiv$ -2.30
Mkn670	14 14 17.5	26 44 41	-	0.061 $\pm$ 0.013	-	520	-	-12.11 $^c$	-	42.27	0.149	-	-	$\equiv$ -2.30
Mkn673	14 17 21.4	26 51 41	0.008 $\pm$ 0.001 $^P$	-	9205	-	-12.32 $^f$	-	42.10	-	0.153	0.598 $\pm$ 0.738	2.33 $\pm$ 1.05	-3.18 $\pm$ 1.27
NGC5929	15 26 07.0	41 40 16	0.013 $\pm$ 0.001 $^P$	-	13356	-	-12.26 $^f$	-	40.83	-	0.208	0.716 $\pm$ 0.498	5.68 $\pm$ 1.16	-2.65 $\pm$ 0.97
NGC5953	15 34 32.5	15 11 39	0.008 $\pm$ 0.001 $^h$	0.065 $\pm$ 0.015	10240	310	-12.25 $^c$	-11.84 $^c$	40.73	41.14	0.343	-	-	$\equiv$ -2.30
NGC6211	16 41 21.5	57 46 24	-	0.008 $\pm$ 0.004	-	817	-	-12.90 $^c$	-	40.99	0.192	-	-	$\equiv$ -2.30
NGC7319	22 36 03.2	33 58 36	0.003 $\pm$ 0.001 $^h$	-	23326	-	-12.46 $^c$	-	41.51	-	0.773	-	-	$\equiv$ -2.30
NGC7674	23 27 57.0	08 46 45	0.023 $\pm$ 0.002 $^P$	-	3881	-	-10.91 $^f$	-	43.33	-	0.531	1.075 $\pm$ 0.598	6.94 $\pm$ 2.19	-4.41 $\pm$ 1.01
NGC7743	23 44 21.4	09 55 57	0.004 $\pm$ 0.001 $^P$	-	18904	-	-13.13 $^f$	-	39.84	-	0.525	$\equiv$ 0.525	1.59 $\pm$ 0.74	-1.83 $\pm$ 1.48

